# UC San Diego
## Oceanography Program Publications

### Title
Multi-model projections of twenty-first century North Pacific winter wave climate under the IPCC A2 scenario

### Permalink
https://escholarship.org/uc/item/65x8k717

### Journal
Climate Dynamics, 40(5-6)

### ISSN
0930-7575 1432-0894

### Authors
Graham, Nicholas E
Cayan, Daniel R
Bromirski, Peter D
et al.

### Publication Date
2012-07-22

### DOI
10.1007/s00382-012-1435-8

### Data Availability
The data associated with this publication are available upon request.

Peer reviewed

eScholarship.org Powered by the California Digital Library
University of California

Clim Dyn (2013) 40:1335–1360
DOI 10.1007/s00382-012-1435-8

# Multi-model projections of twenty-first century North Pacific winter wave climate under the IPCC A2 scenario

**Nicholas E. Graham · Daniel R. Cayan · Peter D. Bromirski · Reinhard E. Flick**

Received: 6 December 2011 / Accepted: 22 June 2012 / Published online: 22 July 2012
© Springer-Verlag 2012

**Abstract** A dynamical wave model implemented over the North Pacific Ocean was forced with winds from three coupled global climate models (CGCMs) run under a medium-to-high scenario for greenhouse gas emissions through the twenty-first century. The results are analyzed with respect to changes in upper quantiles of significant wave height (90th and 99th percentile $H_S$) during boreal winter. The three CGCMs produce surprisingly similar patterns of change in winter wave climate during the century, with waves becoming 10–15 % smaller over the lower mid-latitudes of the North Pacific, particularly in the central and western ocean. These decreases are closely associated with decreasing windspeeds along the southern flank of the main core of the westerlies. At higher latitudes, 99th percentile wave heights generally increase, though the patterns of change are less uniform than at lower latitudes. The increased wave heights at high latitudes appear to be due a variety of wind-related factors including both increased windspeeds and changes in the structure of the wind field, these varying from model to model. For one of the CGCMs, a commonly used statistical approach for estimating seasonal quantiles of $H_S$ on the basis of seasonal mean sea level pressure (SLP) is used to develop a regression model from 60 years of twentieth century data as a training set, and then applied using twenty-first century SLP data. The statistical model reproduces the general pattern of decreasing twenty-first century wave heights south of ~40 N, but underestimates the magnitude of the changes by ~50–70 %, reflecting relatively weak coupling between sea level pressure and wave heights in the CGCM data and loss of variability in the statistically projected wave heights.

**Keywords** Climate change · Ocean waves · North Pacific

N. E. Graham (✉)
Hydrologic Research Center, San Diego, CA, USA
e-mail: ngraham@hrc-lab.org

D. R. Cayan · P. D. Bromirski · R. E. Flick
Scripps Institution of Oceanography,
University of California, San Diego, La Jolla, CA, USA

D. R. Cayan
U.S. Geological Survey, La Jolla, CA, USA

R. E. Flick
California Department of Boating and Waterways,
Sacramento, CA, USA

## 1 Introduction

Ocean wave climate is of obvious importance to coastal and maritime interests, and is a sensitive measure of the impacts of changes in synoptic weather patterns. In the mid-latitude oceans, winter wave climate is determined largely by the strength and favored tracks of migrating low pressure systems. While wind speed in the generation region (the "fetch") is of particular importance, other factors such fetch duration and length are also important, and all are affected by the direction, speed and size of the cyclone. Further, because longer period waves propagate efficiently, changes in cyclone characteristics can affect wave climate at distant locations. Mid-latitude winter wave climate is thus a sensitive integrator of changes in cyclone activity and is one measure of changes in storminess and its effects on other elements of the climate system.

Many studies have examined and compared winter extra-tropical cyclone climatology and variability in reanalysis products and modern climate models. Useful reviews are given by Bengtsson et al. (2006) and Ulbrich

et al. (2009) who describe and compare various techniques used to identify and track extra-tropical cyclones and to characterize cyclone activity. These and other published works provide detailed comparisons of winter cyclone variability in specific models and reanalysis products including Stendel and Roeckner (1998), Alexander et al. (2006), Lambert and Fyfe (2006), Bengtsson et al (2006), Ulbrich et al. (2008, 2009), and Favre and Gershunov (2009). Although the studies cited here use a variety of methods, their results show generally good agreement between the character and amplitude observed and simulated mid-latitude cyclone activity.

Leveraging the agreement between observed and modeled mid-latitude cyclone activity described above, other studies have investigated possible future shifts in North Pacific winter cyclone activity using simulations of twenty-first century climate change (Fischer-Bruns et al. 2005; Yin 2005; Lambert and Fyfe 2006; Bengtsson et al. 2006; Ulbrich et al. 2008, 2009; Favre and Gershunov 2009). A consensus result from these studies is that cyclone activity will decrease south of ~35–40 N, and especially in the western ocean where meridional gradients in cyclone activity are strongest, and will increase north of ~40 N, though there is considerable variability with respect to east–west location of the maximum changes in this latter region.

Questions concerning the character and causes of low frequency variability in wave climate, both past and future, have been addressed previously in several contexts. Interest in the topic was heightened by analyses of wave measurement records from off Britain and Ireland by Carter and Draper (1988) and Bacon and Carter (1991) showing an increasing trend on the order of 2–3 cm year$^{-1}$ in significant wave height ($H_S$) between 1960 and 1985. Similar results for the region were obtained from visual wave observations (Bouws et al. 1996). Later studies using both statistical and numerical models have linked these upward trends to increasing westerly winds associated with a strengthening North Atlantic Oscillation [NAO, see Bacon and Carter 1993; Hurrell 1995; Kushnir et al. 1997; Günther et al. 1998; WASA Group 1998; Wang and Swail 2001, 2002 (henceforth WS2001 and WS2002, respectively); Woolf et al. 2002].

In the North Pacific, routine wave measurements did not begin until the late 1970s and early 1980s, so longer records like those from the eastern Atlantic are not available. Wave model hindcasts (Graham and Diaz 2001; WS2001; Graham 2005) using US National Centers for Environmental Prediction (NCEP) Reanalysis Project (NCEP-RA; Kalnay et al. 1996) winds, and visual wave observations from ships (Gulev and Grigorieva 2004, 2006), indicate substantial upward trends in wave heights over much of the North Pacific south of 40–45 N during the latter half of the twentieth century. These studies relate the upward trends in wave heights to the well-documented expansion of the Aleutian Low and increased westerly winds across the lower mid-latitudes (e.g., Trenberth 1990; Graham 1993; Trenberth and Hurrell 1994; Graham and Diaz 2001; Gulev and Grigorieva 2006). Analyses of buoy measurements from the eastern North Pacific off the North American coast indicate upward trends in wave heights and increasing long-period swell since ~1980 (e.g., Allan and Komar 2000; Bromirski et al. 2005; Ruggiero et al. 2010; see also Gemmrich et al. 2011). These tendencies are qualitatively consistent with visual ship observations (Gulev and Grigorieva 2006), model hindcast results (e.g., Adams et al. 2008), and satellite data (Young et al. 2011).

Other work has considered the possible impacts of anthropogenic climate change on wave climate due to changes in circulation patterns and cyclone characteristics. In an early study, WASA98 used both numerical wave models and statistical approaches to estimate future changes in wave heights over the North Atlantic. For the dynamical approach, a wave model was driven with winds from two 6-year "time slice" simulations performed with a medium resolution (~100 km resolution) global atmospheric model (AGCM) forced with sea surface temperatures from a coupled global climate model (CGCM) in which $CO_2$ concentrations were doubled by ~2050. Bearing in mind that 6-year time slices are very short, the results projected modest increases in wave heights over parts of the northeast Atlantic. The statistical results in the WASA98 study were obtained using a multivariate approach similar to that used by Kushnir et al. (1997) to relate changes in winter mean North Atlantic sea level pressure (SLP) field to quantiles of $H_S$ from a numerical hindcast (Günther et al. 1998), in this case for two reference points in the North Sea. When applied to SLP from two simulations of twenty-first century climate change, the statistical model projected slight increases at the reference locations in one case and slight decreases in the other.

Wang et al. (2004; hereafter WZS2004) also used multivariate regression to relate changes in seasonal mean SLP fields to North Atlantic wave heights (average and 90th percentile). Regression models were trained over 1948–1997 using NCEP-RA SLP and hindcast wave data (see Swail and Cox 2000) and then applied to SLP fields from ensemble climate change simulations with the Canadian CGCM2 model (e.g., Flato and Boer 2001) under three greenhouse gas emission scenarios [the Intergovernmental Panel on Climate Change (IPCC) IS92a, SRES B2 and A2 scenarios (Nakicenovic et al. 2000)]. The results for the higher emission IS92a and A2 simulations give similar patterns of twenty-first century change in North Atlantic wave heights, with increases of 5–35 cm (winter mean $H_S$) in the northeastern North Atlantic and decreases

across the lower mid-latitudes. Much as found for the late twentieth century changes described earlier (e.g., Kushnir et al. 1997; WS2001; WS2002), the projected changes in twenty-first century wave heights were associated with a stronger NAO. Similar results were obtained by Kaas et al. (2001) using a numerical wave model driven with winds from an IS92a simulation with a different CGCM.

Two recent studies have used wave models results in the development of projections of future wave climate in the North Pacific. Cayan et al. (2009) consider the outlook for changes in coastal inundation frequencies for California during twenty-first century using CGCM-derived estimates of sea level and wave climate change. The latter were derived using 6-hourly CGCM winds to drive a numerical wave model (some of these results are used in the present study). The model results exhibited considerable variability of wave energy on interannual to interdecadal time scales, but also showed a tendency for significant wave heights to decline along the southern California coast and to increase along the Northern California coast.

More recently, Mori et al. (2010) describe results from 25-year time slice simulations with a global wave model driven with winds from a very high resolution ($\sim$20 km) atmospheric model forced with ensemble-average SSTs from 18 CGCMs using late 20th (20C3M) and IPCC A1B scenario forcing for the twenty-first century (A1B projects lower emissions than the I92a or A2 scenarios; see also Mizuta et al. 2008). The results comparing late 20th and late 21st conditions show increases in annual average $H_S$ in the northeast Atlantic (up to 5 %) and central North Pacific (up to 2.5 %) poleward of about 40 N and decreases (up to 7 %) between 20 and 40 N (in these regions, the changes are likely dominated by contributions from October to March). For the North Atlantic, these patterns are similar to those described by Kaas et al. (2001) and WS2004.

The discussion above highlights the use of both numerical modeling and statistical approaches in studies of past and future wave climate, a situation that reflects the strengths and drawbacks of each methodology (e.g., Wang et al. 2010). For numerical wave models, some of the drawbacks are purely practical, e.g., they can be time consuming to implement and run, and data storage requirements can be large. Other difficulties are more fundamental. For historical simulations, small changes in observation density and methods, analysis and initialization procedures, and model formulation can result in spurious trends and homogeneities (e.g. WASA98; Wang et al. 2010). For climate changes studies, any problems in the behavior of the climate model from which the wind data are taken will be reflected in the wave model results. On the other hand, many studies have demonstrated that numerical wave models give usefully accurate results for large-scale wave climate studies when suitably implemented with accurate forcing (e.g., Cox and Swail 2001; WS2002; Caires et al. 2004). In contrast to numerical wave models, statistical approaches to wave climate reconstruction have commonly used available time-averaged meteorological fields (e.g., winter mean SLP) that are less vulnerable to the observational and climate model problems noted above. However, as applied here such models generally lose substantial fractions of predictand variance and are subject to artificial skill, so their results are more qualitative and lack the full range of the actual target signal.

In the present paper, we consider possible twenty-first century changes in North Pacific winter wave climate, as characterized by seasonal upper quantile (90th–99th percentile) wave heights, with a numerical wave model driven with winds from three CGCMs using the IPCC SRES A2 emissions scenario (Nakicenovic et al. 2000); A2 is a medium-high scenario in terms of greenhouse gas increases. Additional context is provided by comparisons between CGCM-derived wind and wave climatologies for the modern period with those obtained from reanalysis products. For comparison with numerical wave model results, projections of twenty-first century wave climate change are derived using a statistical approach applied to results from one of the CGCMs in a manner similar to that used in WASA98 and WZS2004. The present study addresses a number of areas pertinent to the development of projections of future wave climate, including techniques for adjusting biases in CGCM near-surface winds, and the comparison of projections made with dynamical and statistical methods. These are among the primary science issues identified for recently initiated efforts towards international coordination of wave projections and intercomparisons (Hemer et al. 2012b).

In the presentation that follows, Sect. 2 describes the climate models and wind data used for the wave model simulations, the wave modeling procedures and analysis methods, and the statistical modeling methodology. Section 3 presents the results from both numerical and statistical modeling results. Section 4 provides a discussion and summary.

## 2 Methods and data

### 2.1 Wave model

The wave model simulations were conducted with the US National Oceanographic and Atmospheric Administration (NOAA) NCEP Wavewatch III (WW3) model, Version 1.18 (Tolman 1999) configured with a spatial resolution of 1.0° × 1.5° latitude–longitude, 5° directional resolution (72 bins), and 20 logarithmically-spaced frequency bins covering the period range from $\sim$4.4 to 27.2 s.

The model domain covers the North Pacific from the coast of Asia to North America (120°E–120°W), and from

20°N to the Aleutian Islands and Alaskan coastline (e.g., Fig. 3a). The domain and spatial resolution are suitable for studies of large-scale boreal winter wave climate in the North Pacific and allows for relatively efficient computation for the multiple centennial-scale simulations used in the present study. A uniform "deep" (>1,000 m) ocean is specified, consistent with the spatial resolution of the model and ocean depths within the model domain. Ocean currents are assumed zero, and neutral atmospheric stability is assumed. Wind data to drive the wave model are supplied at 6-h intervals; model output is produced at 3-h intervals and in the present paper significant wave height ($H_S$) and peak wave direction ($D_P$) are used. For all simulations, reanalysis or CGCM wind data were interpolated bi-linearly from the original spatial resolution to the 1° × 1.5° wave model grid.

The selected model version, domain and spatial resolution for the wave model pose some questions concerning potential limitations; these are discussed below.

1. Why use WW3 v1.18—there are more recent versions of the model? The simulations described in the present paper belong to a larger set of past and future climate change simulations begun using WW3 v1.18 as early as 2003. Version 1.18 was used for subsequent simulations to maintain consistency across the multiple centennial simulations.
2. The southern boundary of the domain is closed at 20°N—how does the affect the results for the upper quantile winter wave heights of concern in this study? During winter, simulated upper quantile (90th–99th percentile) wave heights near the southern boundary are determined almost entirely by large waves generated by mid-latitude storms traversing the Pacific well poleward of 20°N. This point has been verified by comparisons (not shown) between results from near-"twin" simulations, one covering the North Pacific only (as described in the present paper), and the other covering the full Pacific Ocean (the "PWA-R" simulation described in Caires et al. 2004). This latter "all-Pacific" simulation used slightly coarser spatial resolution (1.5° × 2.0°) and had slightly different coastline geometry, but the simulations were otherwise identical with respect to model parameters and NCEP RA wind forcing. Comparisons (not shown, covering 1980–1998) show very close agreement between the results from the two simulations with respect to winter upper quantile wave heights across the entire domain, including near the southern boundary. An exception is in the southwest corner of the "North Pacific-only" domain where the coastlines differ as discussed below.
3. The North Pacific domain is closed along the Aleutian, Kuril and Ryukyu Islands, how does this affect the results? In reality wave energy does filter through gaps in these island chains and has some affect on upper quantile wave heights in the vicinity. (Note that v1.18 of Wavewatch III does not include the parameterization for unresolved islands that appeared with v2.22; Tolman 2003). The closed boundaries along the island chains will result in upper quantile winter wave heights that are somewhat too small in the region near the boundary. Effects on year-to-year variability and the trends described here are likely minor.
4. The Hawaiian Islands are not included in the North Pacific-only domain, what effects does this have? The Hawaiian Islands do affect wave heights in surrounding regions (e.g., see Tolman 2003); during winter the major effect is to shadow the area south and southeast of the islands from swells generated well to the north. As this region is not included in the model domain, the neglected effects of sheltering by the Hawaiian Island for upper quantile winter wave heights within the North Pacific domain is thought to be small.
5. The coarse resolution of the wave model makes for poor resolution of coastal geometry, what effect does this have? The poorly resolved coastlines have greatest effect on waves propagating more or less parallel with the coast, and for these waves can result in unrealistic sheltering immediately along the coast. While the magnitude of these effects are region-dependent, along the coastline of mid-latitude North America most large waves arrive from the west-northwest to west-southwest, so the effect of the coarsely resolved coastline on upper quantile wave heights is expected to be minor for offshore coastal waters, but the model results cannot be considered more than qualitatively representative for protected inshore waters.
6. The model uses a fixed "deep water" depth, what effect does this have? For the spatial resolution and domain used in the simulations described here only a grid cells along the coasts have depths at which interactions with bathymetry become important (~300 m), and these interactions would be very poorly simulated given the coarse resolution of the model. Therefore, and considering the poorly resolved coastlines, modeled wave heights adjacent to coastlines should not be considered as representative of inshore locations on the coast.

### 2.2 Climate models, near-surface wind data and adjustment procedures

This section describes the data sets used to drive the wave model simulations, and the procedures used to adjust the CGCM wind fields.

### 2.2.1 Reanalysis data and climate models

The experiments in this study consist of wave model simulations made using near-surface wind data from a meteorological reanalysis, and from radiatively-forced coupled climate model hindcasts for the late twentieth century and projections of twenty-first century climate. Table 1 provides a synopsis of this information.

*2.2.1.1 NCEP reanalysis* The reference historical wave climate simulation covers 1947–1999 and used 6-hourly 10-m NCEP-RA winds (Kalnay et al. 1996) available at a resolution of $\sim$1.9° latitude–longitude. Results from similar wave hindcasts using NCEP-RA winds with WW3 and with other wave models compare well with buoy and satellite measurements, and with results from simulations using other reanalysis wind sets (e.g., Cox and Swail 2001; WS2001; Graham and Diaz 2001; Caires et al. 2004; Graham 2005).

With specific applicability to the "North Pacific-only" hindcast simulation results used in the present paper, Caires et al. (2004) compared buoy and satellite altimetry measurements with wave heights from the NCEP-RA forced WW-III "full Pacific" simulation described above (Sect. 2.1, Point 2);. Their analyses show good agreement between the WW3/NCEP-RA results and observations, with performance comparable with other hindcast products over the North Pacific. Further, they note that the WW3/NCEP-RA simulation performed particularly well for higher wave conditions. Given the close agreement between the results from the "full Pacific simulation" (analyzed by Caires et al.) and the "North Pacific only" simulation (present paper), the results reported by Caires et al. (2004) bear on the latter simulation as well.

Other verification tests (Graham 2005) compare WW3-RA "North Pacific-only" hindcast results with wave height measurements from four North Pacific NOAA wave buoys in the eastern and central North Pacific (Graham 2005). These comparisons used $>10^4$ contemporaneous 3-hourly model-buoy data pairs for December–March from the late 1970–1998. The hindcast data come from a North Pacific-only simulation identical to that described in the present paper though the western boundary was closed at 150E rather than extending to the coast of Asia. The model-buoy comparisons show very good agreement with correlations of 0.85–0.88 for the 3-hourly data, with little bias at the two exposed buoys in the eastern Pacific [NOAA buoys 46006 (41°N 138°W) and 46026 (38°N 123°W), and slight low biases at a near-coastal buoy off southern California (46011) and buoy 51001 northwest of Hawaii.

*2.2.1.2 NCAR CCSM* Two wave model simulations were conducted using wind data from the NCAR Community Climate System Model (CCSM; version 3.0 beta19), results from which were provided for the IPCC Fourth Assessment) with a spatial resolution of $\sim$1.4° latitude and longitude in the atmospheric model. Near-surface winds are available from the lowest model level ($\sigma = 0.992$) located $\sim$60 m above the surface. General characteristics, performance, and sensitivity of this version of CCSM are discussed by Kiehl et al. (2006) and Collins et al. (2006a, b). Alexander et al. (2006) demonstrate good agreement between CCSM-simulated December–March cyclone track densities over the North Pacific and those from the European Centre for Medium Range Weather Prediction (ECMWF) ERA-40 reanalysis (Uppala et al. 2005).

One CCSM-driven wave model run covers 1941–1999 using winds from a simulation driven with historical solar, volcanic, greenhouse gas and aerosol forcing over the twentieth century (such simulations are designated "20C3M"). A second wave model run covered projected 2000–2099 climate using winds from the CCSM A2 climate change simulation.

*2.2.1.3 CNRM CM3* A second set of wave model simulations (20C3M and A2) used wind data from the Centre National de Recherches Meteorologiques (CNRM) CM3 coupled model (denoted CNRM here; also used for the

**Table 1** Details of wind data sets used in this study (see Sect. 2.2)

| Model | Data used | Spatial resolution | Nominal elevation | Adjustment period | Adjustment factor (10–20 ms$^{-1}$) |
|---|---|---|---|---|---|
| NCEP RA | 1948–1999 | $\sim$1.9° | 10 m | N/A | N/A |
| CCSM 20C3M | 1941–1999 | $\sim$!.4° | $\sim$62 m ($\sigma = 0.992$) | 1970–1999 | −21 to 24 % |
| CCSM A2 | 2000–2099 | As above | As above | As above | As above |
| CNRM 20C3M | 1970–1999 | $\sim$2.8° | 10 m | 1970–1999 | +10 % |
| CNRM A2 | 2000–2099 | As above | As above | As above | As above |
| EH4 A2 | 1990–2099 | $\sim$2.8° | 10 m | 1990–2010 | −5 % |

Spatial resolution and nominal elevation refer to CGCM data as supplied. All wind data were linearly interpolated to 1.0° × 1.5° spatial resolution for use in wave modeling

IPCC Fourth Assessment). For these simulations, CNRM was configured with a spatial resolution of ~1.9° latitude and longitude (interpolated to ~2.8° as distributed); near-surface winds are nominally from 10-m elevation. General aspects of CNRM are described by Salas-Mélia et al. (2005). Kvamstø et al. (2008) demonstrate good agreement between October and March North Pacific cyclone characteristics in the atmospheric component (ARPEGE) of CNRM and those from NCEP-RA. The 20C3M wave model simulation with CNRM covers 1970–1999 and these data were used to initialize the CNRM A2 scenario simulation (2000–2099).

*2.2.1.4 MPI EH4* The third wave model simulation used winds from the Max Planck Institute for Meteorology (MPI) ECHAM4-OPYC CGCM (included in the third IPCC Assessment) and designated here as EH4. EH4 wind data used for the wave modeling come from an A2 scenario simulation covering 1990–2099 (so it began with late twentieth century emissions, and thereafter was driven by projected emissions under the A2 scenario). For this simulation, the ECHAM4 atmospheric component used a resolution of approximately 2.8° latitude and longitude; near-surface wind data are nominally from 10-m elevation. General characteristics and performance of EH4 are described by Legutke and Voss (1999), and Stendel and Roeckner (1998) demonstrate good agreement between winter North Pacific cyclone characteristics in EH4 and ECMWF ERA-15 reanalysis results (Gibson et al. 1997) with the ECHAM4 atmospheric component of EH4 configured at slightly lower resolution (~3.75° × 3.75°) than that used for the A2 simulation described here.

### 2.2.2 *Wind field adjustment procedure*

Prior to performing the final wave model simulations, the CGCM wind fields were adjusted to bring the simulated modern winter (November–March) wave climatologies into better agreement with those obtained using NCEP-RA winds and thus reduce large-scale spatial biases in upper wave height quantiles (90th–99th percentiles) between the CGCM and NCEP-RA results. The adjustment procedure used here casts these biases as resulting from differences in the effective (or nominal) elevation of the near-surface winds, such as might arise from using wind data from well above the surface (e.g., CCSM in this study) or from differences in boundary layer physics. Of course, biases in wind and wave field patterns do not arise only from effective elevation differences, but also from other factors including differences in large-scale circulation patterns and cyclone characteristics, the non-linear response of wave heights to wind speed, among many others. In the context of these factors, the vertical wind profile approach is simply a convenient, physically-based, adjustment method that maintains much of the high frequency space-time structure of the unadjusted fields.

For our work, the wind speed adjustments were made using the boundary layer wind profile model of Liu et al. (1979), and allow the nominal "observation height" windspeed to be adjusted to a desired "reference height" in a manner consistent with the stability, wind-speed and surface roughness. No changes were made to wind direction; neutral stability and a fixed typical marine roughness length were assumed; all changes were applied with reference and observation heights held constant (for a given CGCM) in space and time. Note that although the wind profile-based adjustments are mildly non-linear (with respect to wind speed), for marine wind speeds $> 10$ ms$^{-1}$, and for the range of "observation" and "reference" heights used, the resulting changes in wind speed are small relative to the total wind speed (Fig. 18) and the results are close to being a constant multiple of the original CGCM "observation height" speeds. As a consequence, the temporal and spatial patterns of wind speed variability are approximately conserved. In terms of changes in upper quantile wave height ($H_{99}$), the result of the adjustments to wind speed are approximately linear, as shown by the example for the adjustments applied for EH4 (Fig. 19).

The wind field adjustment procedure used here differs from the more explicit approach used for the numerical model experiments described by Wang et al. (2010). For their time slice (1975–1994, 2080–2099) twenty-first century climate change experiments, the monthly 10-m wind climatologies for 1975–1994 were removed from the climate model wind data and replaced with the corresponding climatologies from the ERA-40 reanalysis. The adjustment procedure also differs from the bivariate quantile mapping method proposed by Hemer et al. (2012a).

The wind speed adjustments for the present work were carried out in two steps for each CGCM. First, the CGCM and NCEP-RA winter wind fields for the late twentieth and early twenty-first century (1970–1999 for CCSM and CNRM; 1990–2010 for EH4) were compared over North Pacific domain, focusing on the 90th and 95th wind speed quantiles. This step provided a general estimate of the reference height adjustment required. After making this initial adjustment, the wave model was run in a series (typically 3–4) of 20–40 year simulations beginning in 1970 (CCSM and CNRM) or 1990 (EH4). After each simulation, the resulting seasonal mean wave statistics were compared with those obtained using NCEP-RA winds for 1970–1999 and adjustments in wind reference height made accordingly, e.g., if wave heights were clearly generally too low, the reference level was moved higher so that the winds supplied to the wave model would be increased. The quality of the wave model results was judged using

subjective comparisons of spatial fields and cross-sections of $H_{90}$ and $H_{99}$, with emphasis on the level of agreement in the central and eastern Pacific between 35 N and 50 N. An objectively optimized adjustment procedure was not employed because these results proved to reasonably balance the CGCM wind and wave climatologies with those derived from NCEP-RA, and because the trial wave model simulations themselves are time consuming. Once the results were deemed satisfactory, the final wave model simulations for that CGCM, including both late twentieth century and entire-twenty-first century periods were performed. Importantly, for a given CGCM, the adjustment function (from the vertical wind profile model) was applied uniformly through time and space across the North Pacific domain through the entire period covered by the wave simulations.

Considering the windspeed range of 10–20 $ms^{-1}$, the final adjustments resulted in 21–24 % windspeed reductions for CCSM (recall the "observation level" wind data for this CGCM come from $\sim$ 60 m elevation), 9–11 % increases for CNRM, and 6–7 % decreases for EH4. The resulting wind and wave climatologies are discussed in Sect. 3 (Figs. 1, 2, 3, 4, 5) (Appendix 2 shows some results regarding the changes in wave heights resulting from the wind speed adjustments for EH4).

## 2.3 Analysis methods

### *2.3.1 Wave model and wind field statistics*

Most results reported here are for November–March ("winter") and for waves focus primarily on 90th and 99th percentile $H_S$ (denoted $H_{90}$ and $H_{99}$, respectively). These quantiles are defined separately for each point and each winter from the population of 3-hourly values of $H_S$ output by the wave model, resulting in annual "maps" of these measures across the North Pacific domain. Results are also given for "associated peak wave direction" ($\mathbf{D}_{99}$), defined here as the vector average of the (unit length) peak wave direction for times when $H_S$ met or exceeded $H_{99}$ for that given winter. Model near-surface winds are treated similarly, but the primary measures are 90th percentile winter wind speed ($WS_{90}$; calculated individually for each grid point from the 6-hourly NCEP-RA or CGCM wind data) and "associated wind components" ($\mathbf{U}_{90}$) defined as the vector average wind velocity for cases where the 6-hourly wind speed met or exceeded the value $WS_{90}$ for that winter.

Additional results are reported for the average of the five largest peak significant wave heights during each year (designated $H_{PK5}$). For this statistic, a "peak" significant wave height event is defined as the maximum height such that no larger peak occurs within 36 h before or after the time of the peak. This definition is designed to isolate peak wave heights associated with individual "storm" episodes and the statistic has been used some recent analyses of trends in measured (buoy) wave heights from the northeast Pacific (e.g. Ruggiero et al. 2010; Gemmrich et al. 2011).

### *2.3.2 Statistical projections*

Developing centennial-scale data sets with numerical wave models is computationally demanding and realistic results require accurate (or realistic) wind data with few biases or inhomogeneities. Because such wind data are not available for most of the first half of twentieth century, and because winds from,many CGCM climate change simulations were not saved at the necessary temporal granularity and thus are unsuitable for numerical wave modeling (see WASA98; WZS2004; Wang et al. 2010), there has been considerable interest in developing statistical methods. These methods typically estimate seasonal wave statistics on the basis of large-scale, time averaged atmospheric fields, most frequently seasonal average sea level pressure (SLP). Such approaches take advantage of the known associations between variability in large-scale circulation patterns and changes in mid-latitude cyclone characteristics (tracks, strength; e.g., Lau 1988; Chang and Fu 2003; Zhu et al. 2007), and have been shown to be useful in a variety of contexts (e.g., Kushnir et al. 1997; WASA98; WS2001; WS2002; Bromirski et al. 2005; WZS2004).

The statistical methodology used in the present work closely follows that used by WASA98, WS2001, WS2002 and WZS04 for reconstructions and diagnostics of twentieth century wave climate, and projections for twenty-first century for the North Atlantic (WASA98; WS2004). This approach ("PC regression"; e.g., Hotelling 1957; Kendall 1957; Jolliffe 2002; see "Appendix 1") involves development of linear regression models linking the time functions (or "PC's") of the Empirical Orthogonal Functions (EOFs) of seasonal average SLP (the predictor; usually from operational analyses or reanalysis results) and an upper quantile of seasonal wave height (the predicatand, e.g., 90th percentile wave height) from a wave model hindcast driven with winds from analyses or reanalysis data sets. Typically, the training period for these regression models covers a few decades of the late twentieth century. The method has been applied in various contexts in many studies related to climate diagnostics and prediction (e.g., Horel 1981; Barnett et al. 1993). When augmented to provide additional information about the spatial and temporal structures underlying the model's predictability, the method is known as "Redundancy Analysis" (RDA; Tyler 1982; von Storch and Zweirs 1999); note these additional steps do not alter the form of the regression model itself, or its performance. RDA was used in the studies of WASA98, WS2001, WS2002 and WZS04 cited earlier. Kushnir et al.

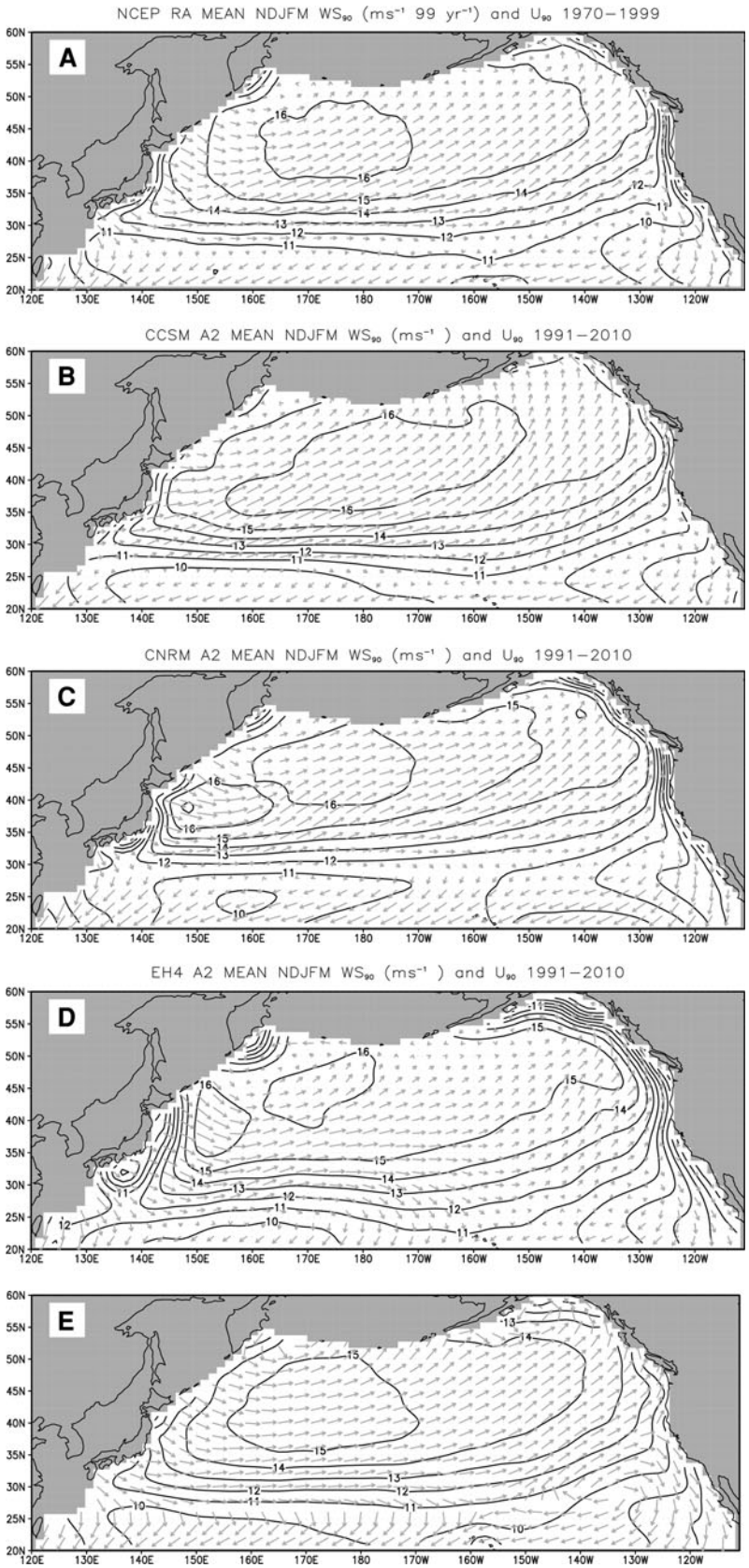


**Fig. 1** Average of November-March $WS_{90}$ ($ms^{-1}$) and $\mathbf{U}_{90}$ for **a** NCEP-RA (1970–1999), **b** CCSM-A2, **c** CNRM-A2, **d** EH4-A2 (all for 1991–2010); for clarity, vectors are fixed length and show direction of $\mathbf{U}_{90}$ (magnitude is given by $WS_{90}$), **e** winter average $WS_{90}$ ($ms^{-1}$) and $\mathbf{U}_{90}$ for ERA-40 (1970–1999). CGCM results use adjusted wind data (see Sect. 2.2.2)

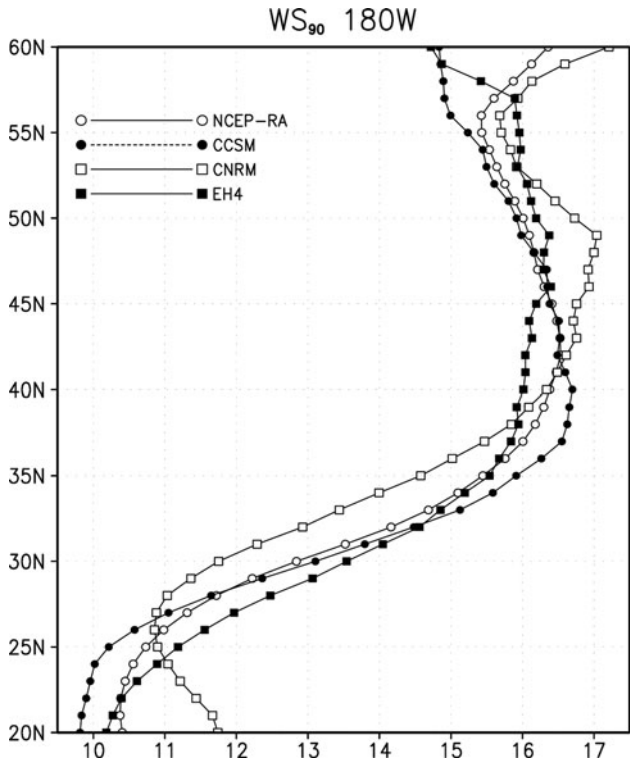


**Fig. 2** Average $WS_{90}$ ($ms^{-1}$) along 180 W as a function of latitude for NCEP-RA (1970–1999; *open circles*), and for 1991–2010 for CCSM-A2 (*filled circles*), CNRM-A2 (*open squares*), and EH4-A2 (*filled squares*)

(1997) used a closely related method (Canonical Correlation Analysis) in their diagnostic study of trends in North Atlantic wave climate.

In the present work, PC regression models were developed to emulate an application to a "real world" situation, but using CCSM results as a surrogate climate. The model was trained using seasonal mean SLP (the predictors) and simulated seasonal $H_{90}$ and $H_{99}$ (the predictands; separate models were derived for $H_{90}$ and $H_{99}$) from 20C3 M results over the winters 1940–1941 to 1999–2000 (60 years; CCSM A2 results filled out January–March 2000). The derived regression models were then applied using SLP data from the CCSM A2 results for 2000–2001 to 2098–2099 (99 years) to obtain statistical projections of $H_{90}$ and $H_{99}$. The statistical estimates are compared with actual $H_S$ quantiles from the numerical modeling to evaluate the performance of this statistical method, for this particular CGCM and scenario. As applied, the methodology uses a "perfect model" approach in which one has error-free seasonal mean SLP and wave-quantile fields for 1941–2000 with which to construct statistical models, error-free projections of twenty-first century SLP with which to drive them, and after-the-fact perfect wave-quantile fields against which to test the results.

An important free parameter in PC regression is the number of EOF modes (M) to be retained for the predictor and predictand fields. As M is increased, the hindcast performance of the model will invariably increase, but because some of this increase in performance is due to over-fitting ("false skill"), actual (or cross-validated, as in WS2001) performance will begin to decrease at some point. For the present work, M was varied over the range of 2–15 modes, with separate regression models fitted for each. The performance of the resulting models was evaluated by comparing the statistically-derived results for the twenty-first century with those obtained from the wave model (the "actual" results), as described in the section below.

### 2.3.3 Statistical measures

For both numerical wave model results and the statistical projections, the measure of change during the twenty-first century is the difference ($\Delta$) between 30-year mean quantiles of winter wave height or wind speed for 2070–2099 less those for 2001–2030. The significance of these differences is assessed using the usual *t* test (for difference in means; Sokal and Rohlf 1969).

For the performance of the statistical models, we use "pattern skill" ($S_{PAT}$) as the primary figure of merit to compare the statistically-derived and modeled 30-year difference fields ($\Delta$, see above), where

$$S_{PAT} = 1 - \left[\langle e^2\rangle \langle z^2\rangle^{-1}\right]$$

with

$$\langle e^2\rangle = N^{-1}\sum\left[(\Delta_{STAT} - \Delta_{NUM})^2\right]$$
$$\langle z^2\rangle = N^{-1}\sum\left[\Delta^2_{NUM}\right]$$

Here, N is the number of grid points, $\Delta_{STAT}$ and $\Delta_{NUM}$ are the difference maps for the numerical and statistical results, respectively, and the summation is over the locations in the wave model domain.Also reported is the pattern correlation ($R_{PAT}$)

$$R_{PAT} = C_{YZ}(C_{YY}C_{ZZ})^{-1/2}$$

where

$$C_{YZ} = N^{-1}\sum \Delta'_{NUM}\Delta'_{STAT}$$
$$C_{YY} = N^{-1}\sum \Delta'_{NUM}\Delta'_{NUM}$$
$$C_{ZZ} = N^{-1}\sum \Delta'_{STAT}\Delta'_{STAT}$$

with $\Delta$' indicating the spatial average has been removed from the difference map.

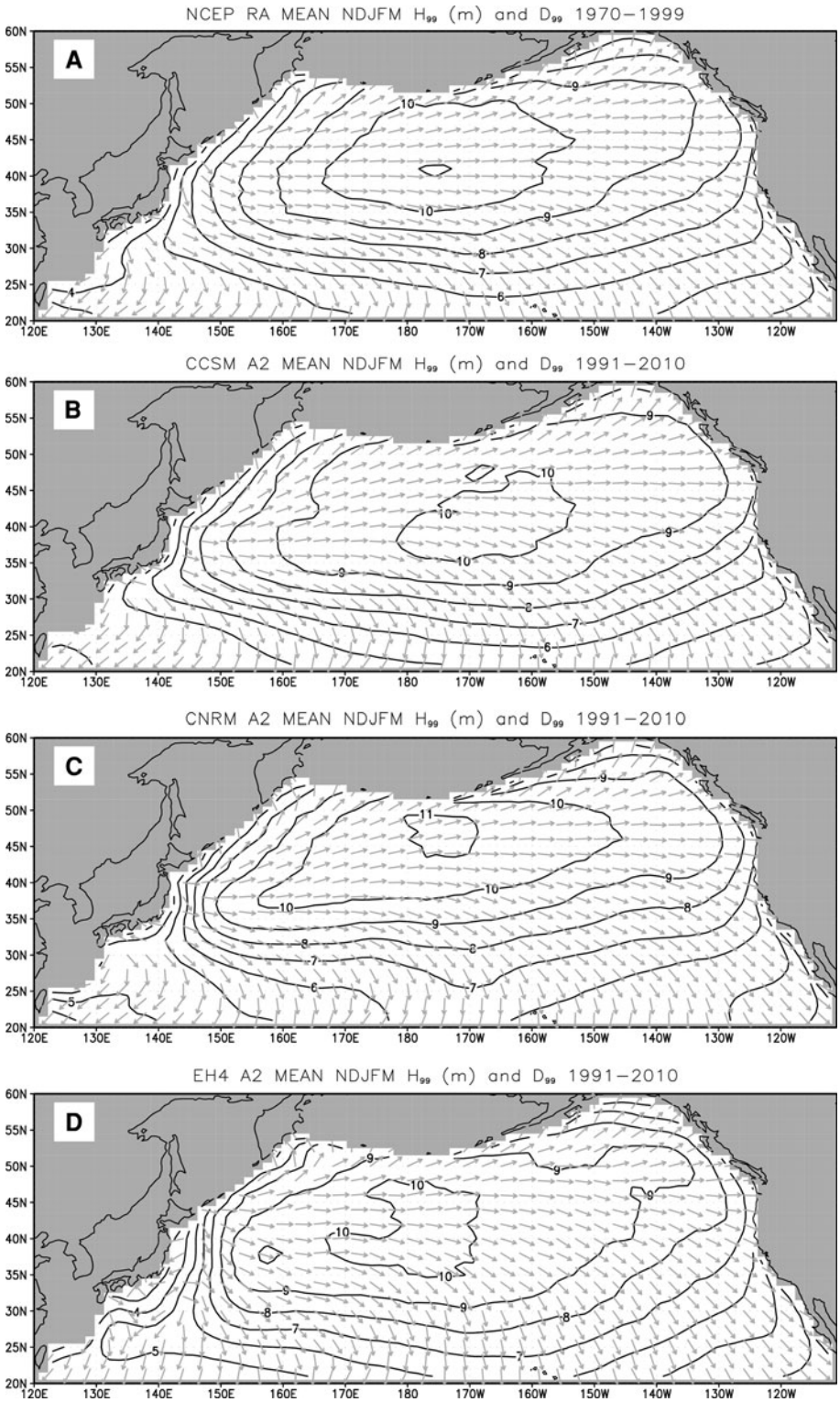


**Fig. 3** Winter average $H_{99}$ (m) and $\mathbf{D}_{99}$ for **a** NCEP-RA (1970–1999), **b** CCSM-A2, **c** CNRM-A2, and **d** EH4-A2 (all for 1991–2010)

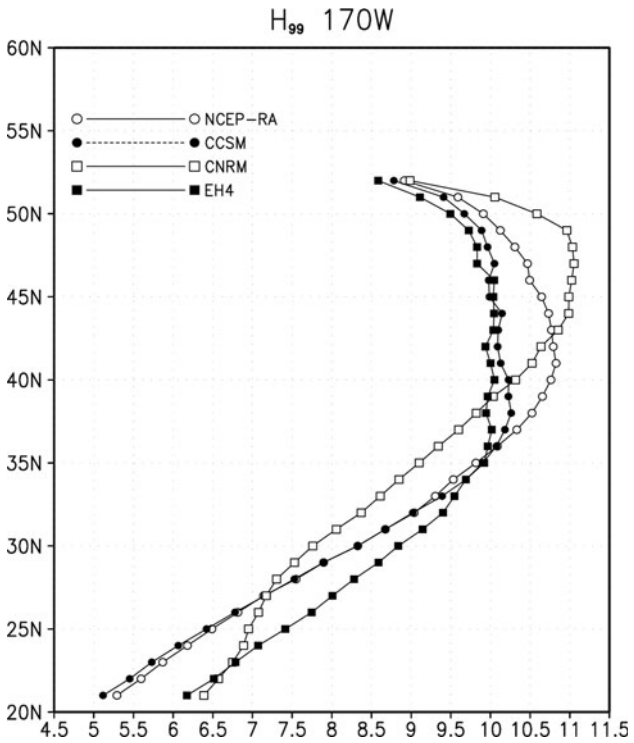


**Fig. 4** Winter average $H_{99}$ (m) along 170 W as a function of latitude for NCEP-RA (1970–1999; *open circles*), and for 1991–2010 for CCSM-A2 (*filled circles*), CNRM-A2 (*open squares*), and EH4-A2 (*filled squares*)

## 3 Results

### 3.1 Wind and wave climatologies

Climatologies of near-surface winds (November–March $WS_{90}$ and $\mathbf{U}_{90}$) from the NCEP-RA (1970–1999) and CGCM results (1991–2010; CGCM winds are post-adjustment—see Sect. 2.2.2) are shown in Fig. 1. The large-scale features in the climate model results show qualitative agreement with the observations (compare Fig. 1a with b–d) in showing a broad maximum stretching from ~35 to 40 N latitude in the western ocean to about 50 N in the eastern Gulf of Alaska, with peak speeds of about 16 $ms^{-1}$ in west-southwesterly flow centered just west of the dateline. For the 20-year comparison period, a clear discrepancy in the CNRM and EH4 results (Fig. 1c, d, respectively) is that both show separate wind maxima (up to 16 $ms^{-1}$) in the far western Pacific that do not appear in either the NCEP-RA or CCSM results (Fig. 1a, b, respectively). The CNRM and EH4 fields also have much lower wind speeds near land in the northeastern Gulf of Alaska than either the NCEP-RA or CCSM results.

To document that the NCEP-RA winds provide a representative standard for comparison, Fig. 1e shows winter $WS_{90}$ and $\mathbf{U}_{90}$ for the ERA-40 reanalysis for 1970–1999. The NCEP-RA and ERA-40 results agree closely in terms of pattern though the ERA-40 90th percentile wind speeds are systematically lower by ~5 %, giving a discrepancy of ~0.7–0.8 $ms^{-1}$ through the core of the westerlies. A tendency for a low bias in the ERA-40 winds over the northeast Pacific was also noted by Caires et al. (2004) who found that ERA-40 mean wind speeds averaged ~0.5 $ms^{-1}$ below those measured at four NOAA buoys, and ~0.4 $ms^{-1}$ below the corresponding averages from NCEP-RA results. For comparison, the gridded data sets used here yield a difference in domain-averaged mean wind speed of 0.38 $ms^{-1}$ (NCEP-RA less ERA-40, 1970–1999). Results from wave model simulations (identical model configuration as described here) using ERA-40 winds (not shown) indicate that the lower ERA-40 10-m windspeeds (relative to NCEP-RA) may be a primary cause of the low bias in upper quantile: ERA-40 hindcast wave heights (relative to TOPEX measurements) documented by Caires et al. (2004; their Fig. 2).

In terms of the meridional distribution of high quantile winds (Figs. 1, 2), the westerlies in the CCSM extend slightly too far south through the central ocean, a tendency that is more exaggerated in the EH4 climatology. In contrast, in the CNRM results, the central Pacific westerlies are located about 5° too far north, a discrepancy that extends into the eastern ocean. These general features and discrepancies are robust and appear in the CGCM climatologies for the full twenty-first century as well (not shown).

For simulated November–March $H_{99}$ and $\mathbf{D}_{99}$ (Fig. 3a–d), the CGCM climatologies for 1991–2010 show general agreement with the NCEP-RA results for 1970–1999, and features that are closely related to those noted for the surface wind climatologies. All the results show maxima in $H_{99}$ of 10–11 m between approximately 35–50 N and 170E–155 W embedded within a broad region of higher waves (coming predominantly from the west) oriented from west-southwest to east-northeast across the North Pacific from the coast of Japan into the Gulf of Alaska. The wave height maxima (and general patterns) tend to be displaced 10–15° east (i.e., downwind) of the wind speed maxima, reflecting the efficient generation of and eastward propagation of waves along the southern side of migrating mid-latitude cyclones (so that the largest waves tend to be found near eastern end of the favored regions for strong westerly fetches).

While the propagation of swell and complexity of the wave generation processes limit the relevance of pointwise comparisons between wind speed and wave height climatologies, many of more obvious differences between the NCEP-RA and CGCM-based $H_{99}$ climatologies can be related to differences in their respective $WS_{90}$ climatologies. For example, the excessive wave heights in the CNRM and EH4 results (relative to NCEP-RA) over the mid-latitude far western Pacific are very likely due

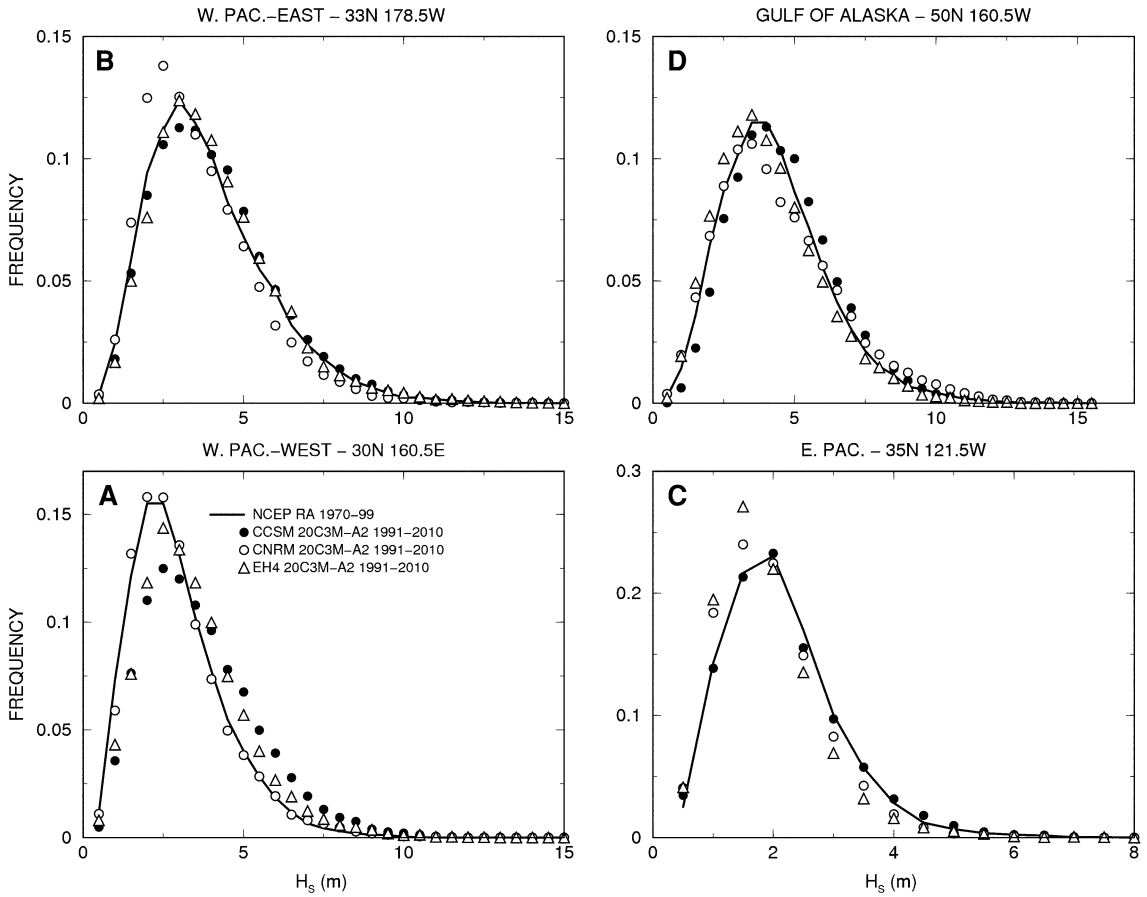


**Fig. 5** Frequency distributions winter $H_S$ for model grid points at **a** 30 N 160.5E, **b** 33 N 178.5 W, **c** 35 N 121.5 W and **d** 50 N 160.5 W. Data are for NCEP-RA (1970–1999; *solid line*), and combined 20C3 M and A2 results for 1991–2010 for CCSM (*closed circles*), CNRM (*open squares*) and EH4 (*open triangles*)

the excessive CGCM wind speeds in that region. In the central North Pacific, longitudinal sections along 170 W (Fig. 4) show a pronounced ~5° northward shift of the main features of the CNRM $H_{99}$ climatology, broadly consistent with the comparable displacement mean $WS_{90}$ field (Fig. 2). Likewise, the excessive equatorward extent of the westerlies south of 30 N in the EH4 results (Figs. 1, 2) is reflected in the $H_{99}$ climatology as well (Figs. 3, 4).

To give a further idea of how well the CGCM wave climate compare with the NCEP-RA results, Fig. 5 shows frequency distributions of winter wave heights at grid points in the (a) far western and (b) west-central lower mid-latitude Pacific, (c) eastern North Pacific off central California, and (d) in the western Gulf of Alaska. Although there are some clear discrepancies, particularly in the western ocean (Fig. 5a) where the CCSM and EH4 results are skewed towards higher values, the agreement between the distributions is relatively close indicating that the CGCM wave results capture the main features of the regional wave climates.

Overall, the CCSM results appear to be in best agreement with the NCEP-RA data in terms of both mean winter $WS_{90}$ and $H_{99}$ for modern decades. At the same time, although the CNRM and EH4 results show some marked discrepancies, the dominant features in the reanalysis results are well replicated, supporting the notion that meaningful interpretations can be made of the simulated changes in North Pacific wave climate through the twenty-first century.

### 3.2 CGCM simulated twenty-first century wave climate

Turning now to the results for the twenty-first century, Fig. 6 shows differences between 30-year average winter $H_{99}$ (2070–2099 less 2001–2030) from the A2 scenario wave model simulations. The difference maps show notably similar patterns of change, with decreases in wave heights south of 40–45 N and increases to the north. For each model, the decreases in $H_{99}$ are largest (0.75–1.5 m; ~10–15 % of the 2001–2030 mean) and most widely statistically significant in the western and central Pacific. Projected decreases in $H_{99}$ are smaller in the lower mid-latitudes of the eastern Pacific, with decreases up to 0.25–0.50 m (5–10 %) that are near the 95 %

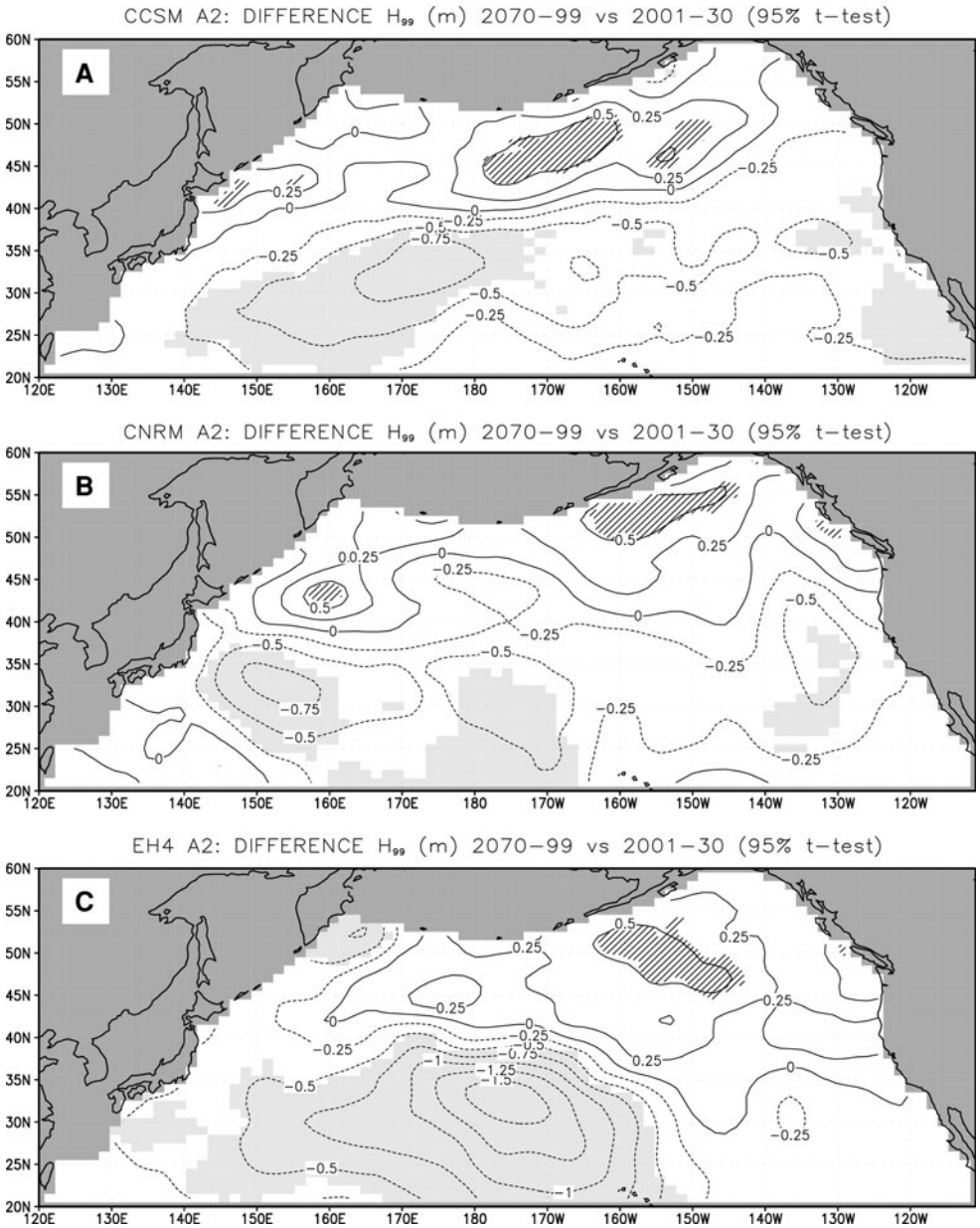


**Fig. 6** Differences (m) in simulated winter average $H_{99}$ (2070–2099 less 2001–2030) for **a** CCSM-A2, **b** CNRM-A2, and **c** EH4-A2. *Shading* (*hatching*) indicates where differences exceed the *t* test 95 % confidence limit

significance limit for CCSM and CNRM, while the EH4 results show smaller (<0.25 m), non-statistically significant decreases. Only the EH4 results indicate statistically significant declines (>0.5 m) in wave heights around the Hawaiian Islands, with CCSM and CNRM showing smaller and non-significant decreases. In the northern Pacific, projected increases in $H_{99}$ range up to 0.5 m (~5 %), and each model indicates the largest and most significant changes reaching from south of the eastern Aleutian Islands towards the coast of North America. There is little consistent agreement between the model results in the far northwestern Pacific, though each model shows some increases in the region.

Immediately along the coast of North America, all of the model results indicate a pattern of increased wave heights in the north and decreases to the south, with the latitude of the transition between these regimes differing considerably from model to model (farthest north in CCSM and farthest south in EH4). Both the CCSM and CNRM results indicate decreasing wave heights (up to 0.4 m) south of ~45 N, but these are statistically significant only in CCSM. In contrast, both CNRM and EH4 show increasing wave heights (up to ~0.3 m) along the coast of western Canada and eastern Alaska; these changes pass (barely) the 95 % significance test off southern British Columbia.

Figure 7 shows twenty-first century changes for $H_{90}$. South of 40–45 N, the patterns of changes are similar to those for $H_{99}$ (Fig. 6) but slightly smaller in magnitude, with statistically significant decreases up to 0.5–0.75 m concentrated in the west-central Pacific. As with the $H_{99}$ results, the decreases in this region are largest in the EH4

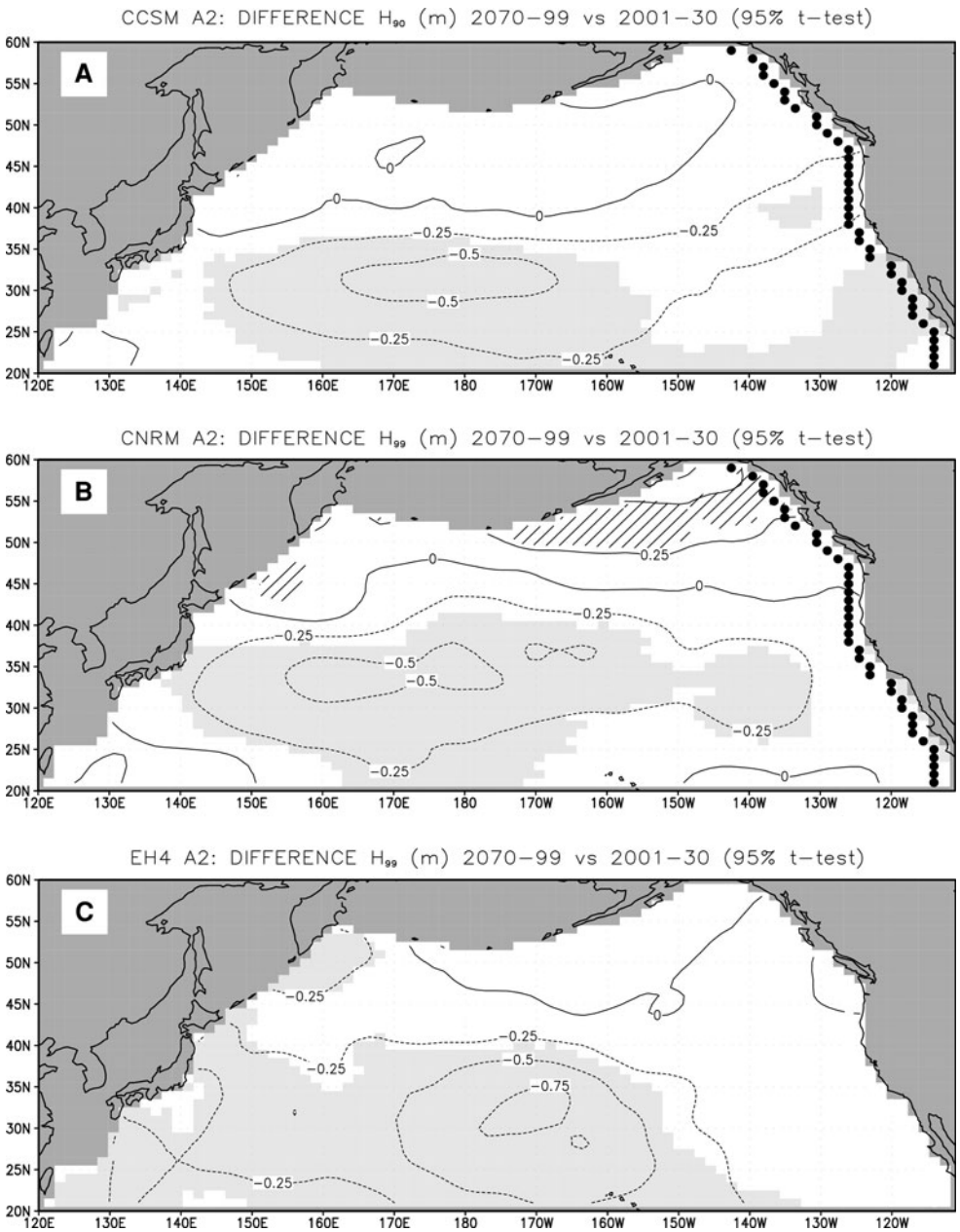


**Fig. 7** Differences (m) in simulated winter average $H_{90}$ (2070–2099 less 2001–2030) for **a** CCSM-A2, **b** CNRM-A2, and **c** EH4-A2. *Shading* (*hatching*) indicates where differences exceed the *t* test 95 % confidence limit. *Black circles* in *upper panel* (**a**) mark locations of points used for western North America profiles in Fig. 17

results, and extend farther east in the CCSM and CNRM results. At higher latitudes the patterns of change in $H_{90}$ again show widespread increases, though for CCSM and EH4 these increases are relatively small (<0.25 m) and not statistically significant. For CNRM, the $H_{90}$ change results in this region are more similar to their $H_{99}$ counterpart, with statistically significant increases of up to ~0.25 m across parts of the Gulf of Alaska.

As the changes in projected wave climate ultimately derive from changes in surface winds, it is not surprising to find points of correspondence between 21st changes in simulated $WS_{90}$ and $\mathbf{U}_{90}$ (Fig. 8a–c) and those for $H_{99}$ and $H_{90}$ (Figs. 6, 7). The results for each model show statistically significant declines of ~0.75–1.0 $ms^{-1}$ (~5–7 %) in $WS_{90}$ across the lower latitudes of the central and western Pacific approximately collocated with the largest declines in $H_{99}$ and $H_{90}$. The similarity in the patterns of windspeed change in this region is particularly marked for the CCSM and CNRM results (Fig. 8a, b). For these models, the decreases concentrated in a zonally oriented band between about ~25–38 N between the Asian coast and ~165 W, with the $\mathbf{U}_{90}$ differences showing that the decreasing windspeeds result primarily from slackening winds along the southern flank of the mean westerlies (see Fig. 1c, d). A similar correspondence in wave and wind changes is found in the EH4 results in the region of the low latitude westerlies (Fig. 8c), though in this case the largest decreases in windspeeds are located farther south than in

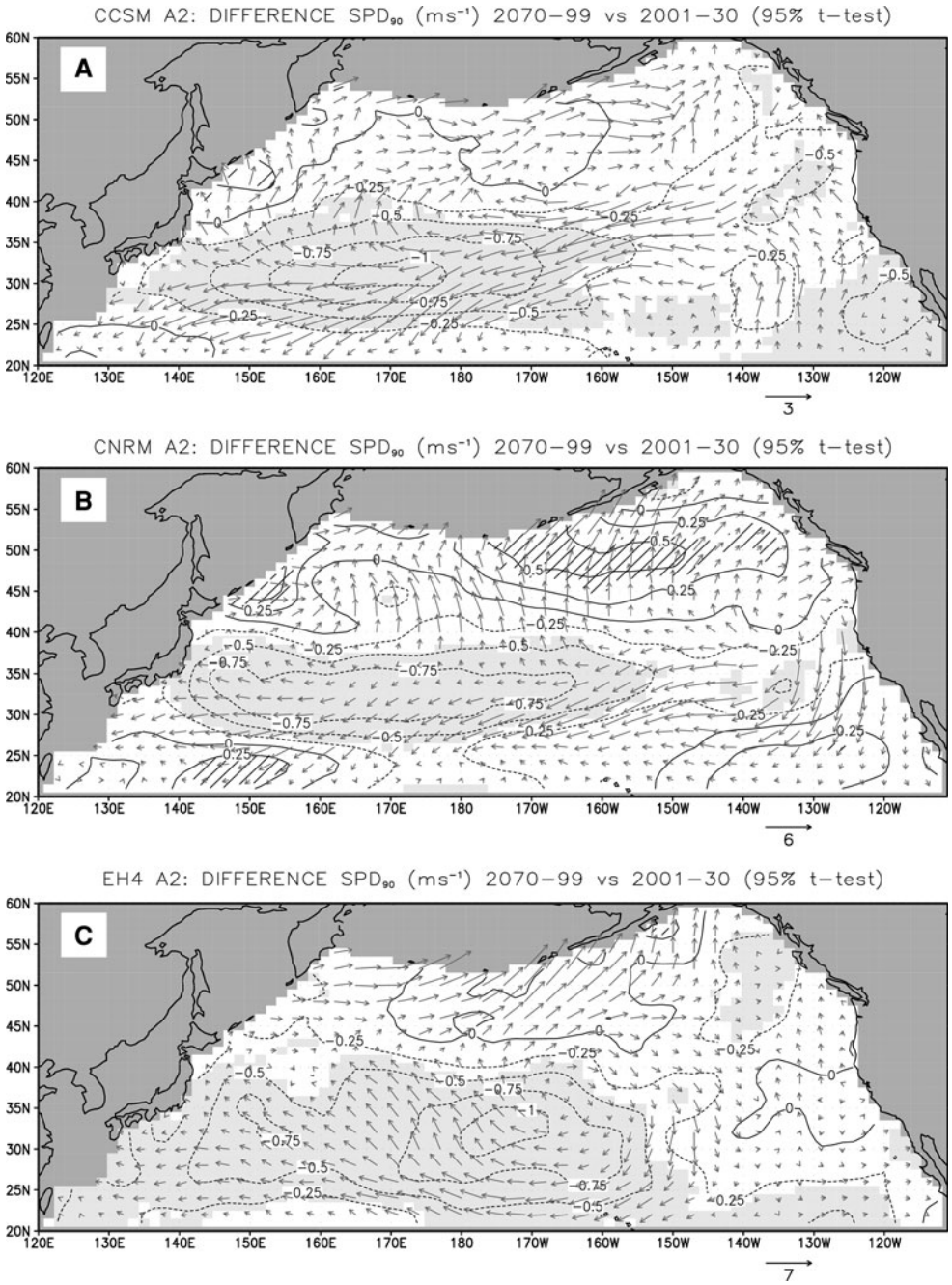


**Fig. 8** Simulated differences ($ms^{-1}$) in winter average $WS_{90}$ and $\mathbf{U}_{90}$ for 2070–2099 less 2001–2030 for CCSM-A2 (**a**), CNRM-A2 (**b**), and EH4-A2 (**c**). *Shading* (*hatching*) indicates where differences exceed the *t* test 95 % confidence limit. Note difference in vector scaling (*lower right in each panel*)

CCSM and CNRM (extending down to 20 N), consistent with the more southward extent of the average westerlies in this model (Fig. 1d). In the eastern Pacific, the simulated changes $WS_{90}$ in the CCSM and CNRM results both show widespread decreases, though the patterns of change in $\mathbf{U}_{90}$ are quite different, while the EH4 results show a more mixed pattern of regional changes.

At latitudes north of 45–50 N, the relationship between simulated changes in $H_{99}$ and $WS_{90}$ are not as systematic as those at lower latitudes discussed above. In particular, while both the CCSM and EH4 (Fig. 8a, c) results show significant increases in $H_{99}$ of >0.5 m, there are only minor changes in $WS_{90}$, with the $\mathbf{U}_{90}$ changes showing increasing components from the west to southwest. In contrast, the CNRM wind changes (Fig. 8b) do show statistically significant increases in both $H_s$ and wind speed (0.5 $ms^{-1}$, ~3 %), apparently resulting mostly from increased southerly components. For CCSM and EH4, the increases in $H_{99}$ in this region may reflect systematic changes in the spatial and temporal organization of the wind fields associated with stronger low pressure systems. Notably, the simulated twenty-first century changes in $WS_{90}$ for CCSM and EH4 agree much better with the changes in $H_{90}$ (Fig. 7) than with $H_{99}$ (Fig. 6). An examination of changes

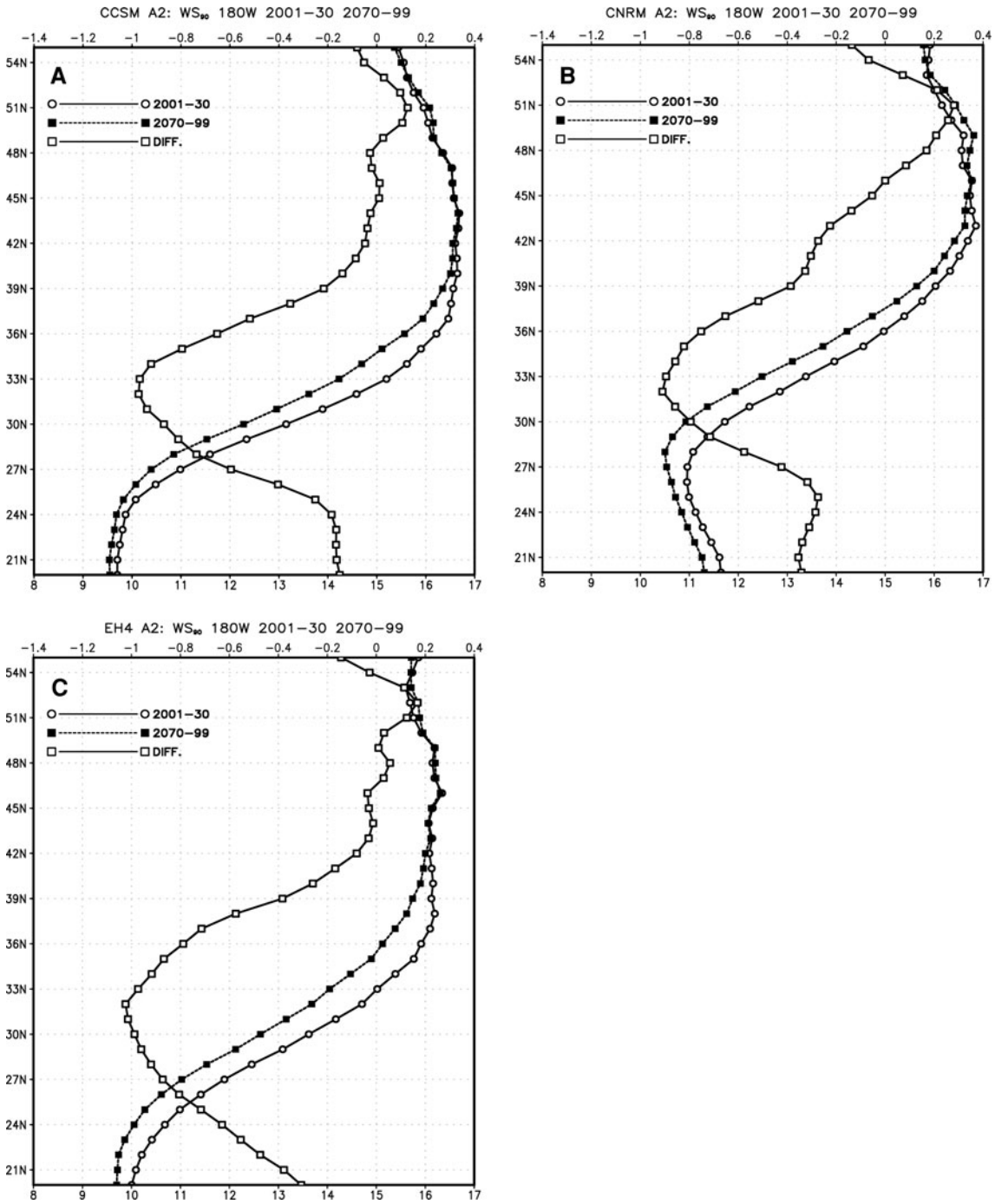


**Fig. 9** Cross-sections along 180 W of November–March average $WS_{90}$ ($ms^{-1}$; lower abscissa) for 2001–30 (*open circles*), 2070–99 (*filled squares*), and their difference (later period—earlier period; *open squares*; upper abscissa); results for **a** CCSM-A2, **b** CNRM-A2, **c**EH4-A2

in winter 99th percentile windspeeds (not shown, and note that the 6-h sampling time for these data is rather crude for such a high quantile) shows somewhat better agreement with the $H_{99}$ changes, but it is plausible that other factors at play may involve more subtle changes in the wind environment, e.g., a northward shift in the favored track of maturing cyclones in the latter part of the twenty-first century.

Figure 9a–c show meridional sections of average $WS_{90}$ along 180 W for 2001–2030 and 2070–2099, and their difference, for CCSM, CNRM and EH4, respectively. As noted earlier, in each model the decreases in windspeed are confined to the region south of the strongest westerlies, with the largest changes, approximately 1 $ms^{-1}$ at this longitude, located between ~31 and 35 N. These findings, along those in Fig. 8, emphasize that the widespread

decreases in simulated twenty-first century $H_{99}$ and $H_{90}$ across the lower mid-latitude North Pacific result primarily from a reduction in the westerlies south of their main axis, rather than from a northward shift of the general wind pattern through all longitudes.

### 3.3 Statistical downscaling

Hindcast and twenty-first century projection results for the statistical modeling of CCSM $H_{99}$ and $H_{90}$ (Sect. 2.3.2, Appendix 1) using CCSM model SLP are summarized in Table 2. As described earlier, the regression models were developed over 1941–2000 (the hindcast or calibration period) using 20C3 M results (winter mean SLP as the predictor, winter $H_{90}$ and $H_{99}$ as the predictand) and then applied through the twenty-first century using A2 winter mean SLP (anomalies from the 1941–2000 climatology) to drive the regression model. A similar exercise was conducted using NCEP-RA SLP and associated WW3 wave quantiles over 1949–1999. The NCEP-RA results are used for comparison purposes and verify we obtained results consistent with those of WS2001. Considering first the hindcast results and referring to Table 2, note that while the fractions of variance of captured by the first few EOFS of SLP and wave heights are similar for the CCSM and NCEP-RA results, the redundancy index (RI), and resulting $R^2$ (given the similar efficiency of the EOF analyses) are considerably lower for the CCSM-derived values, $\sim$40–50 % less for $H_{99}$ and $\sim$30 % less for $H_{90}$. [Note: our NCEP-RA hindcast results are somewhat more skillful (higher fractions of variance, RI and $R^2$) than those obtained by WS2001 in a similar analysis (for M = 7) covering January–March 1958–1997, and using results form a different wave model and different SLP data set.].

To give an idea of how the statistical models perform on a spatial context, Fig. 10a, b show pointwise correlations between statistically-derived and modeled hindcast $H_{90}$ (M = 7) for NCEP-RA and CCSM, respectively. The correlation patterns are quite similar, with the highest values centered along $\sim$35–40 N in the central and eastern North Pacific, and much more broadly distributed in latitude off the coast of North American than off Asia, reflecting the impact of variability in the seasonal strength of the Aleutian Low and mid-latitude westerlies across the central Pacific (e.g., WS2001) and resulting wave generation and propagation into the eastern ocean. As expected from the $R^2$ values in Table 2, the correlations for the NCEP-RA results are notably higher than those for CCSM.

We have not analyzed in detail why the hindcast performance for CCSM and NCEP-RA differ so markedly, but the fact that the EOFs in two analyses capture similar fractions of variance while the RI values are quite different shows that reason lies with weaker statistical coupling between seasonal SLP and wave height fields in the CCSM results as compared with those from NCEP-RA. Some

**Table 2** Hindcast (left side) AND projection (right side) statistics for November–March CCSM-A2 $H_{99}$ and $H_{90}$

| M | $H_{99}$ hindcast | | | | Projection | |
|---|---|---|---|---|---|---|
| | $F_{var}$ SLP | $F_{var}$ $H_{99}$ | RI | $R^2$ | $S_{PAT}$ | $R_{PAT}$ |
| 4 | 0.881 | 0.543 | 0.312 | 0.169 | 0.083 | 0.449 |
| | (0.888) | (0.610) | (0.594) | (0.362) | | |
| 7 | 0.944 | 0.672 | 0.339 | 0.228 | 0.058 | 0.390 |
| | (0.955) | (0.729) | (0.546) | (0.398) | | |
| | [0.893] | [0.630] | [0.482] | [0.300] | | |
| M | $H_{90}$ hindcast | | | | Projection | |
| | $F_{var}$ SLP | $F_{var}$ $H_{90}$ | RI | $R^2$ | $S_{PAT}$ | $R_{PAT}$ |
| 5 | 0.909 | 0.731 | 0.479 | 0.350 | 0.173 | 0.568 |
| | (0.926) | (0.809) | (0.693) | (0.561) | | |
| 7 | 0.944 | 0.796 | 0.493 | 0.392 | 0.065 | 0.455 |
| | (0.955) | (0.858) | (0.683) | (0.586) | | |
| | [0.893] | [0.767] | [0.587] | [0.450] | | |

Results for statistical models [specified by number of retained EOF modes (M)] giving the best projection performance in terms of pattern skill

$F_{var}$ gives the fraction of original variance retained in the EOFs; RI is fraction of total retained by the EOFs; $R^2$ is fraction of total original variance retained after regression (or "redundancy index" following WS2001); $S_{PAT}$ and $R_{PAT}$ are pattern skill and pattern correlation between modeled (Figs. 6, 7) and statistically-derived (Figs. 11, 12) 30-year difference maps. Values in parentheses are for NCEP-RA hindcast results for 1948–1949 to 1998–1999 (51 years). Values in brackets are from WS2001 (their Table 1) for January–March 1958–1997 (40 years). CCSM-A2 hindcast results are for 1940–1941 to 1999–2000 and projection results for 2001–2099

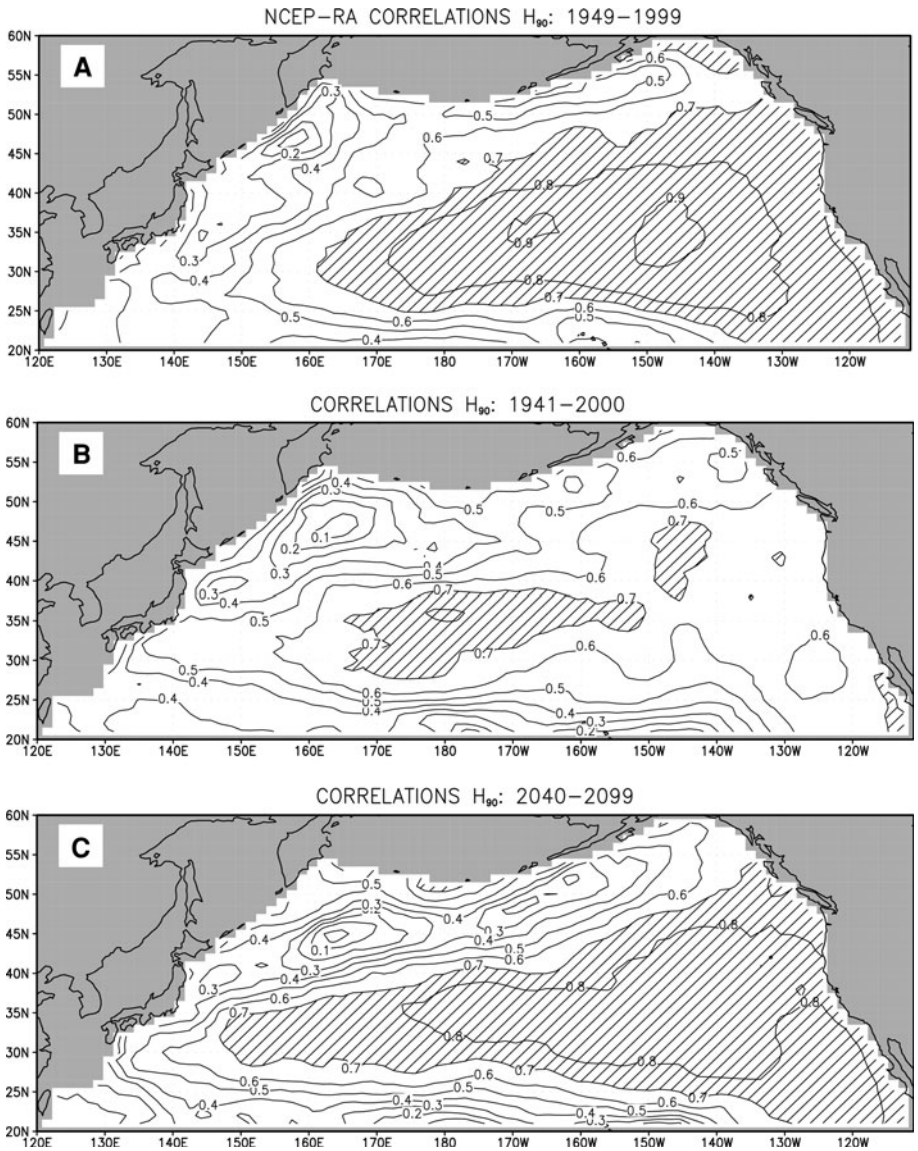


**Fig. 10** Correlations between modeled and statistically-derived $H_{90}$ (M = 5) for **a** NCEP-RA hindcast, 1948–1999; **b** CCSM-20C3 M hindcast $H_{90}$, 1941–2000, and **c** CCSM-A2 projection; 2040–2099. Values over 0.7 are *hatched*

possible causes include (1) differences in the characteristics of cyclones (and associated episodes of strong winds) and their relation to the seasonal mean SLP field, (2) the use of scaled lowest model level ($\sigma = 0.985$) winds, rather than 10-m winds for the CCSM wave modeling, and (3) somewhat weaker ENSO-related SLP and wave height variability over the North Pacific in CCSM (not shown).

Turning to the statistical projections for the twenty-first century, the statistically-derived 30-year differences (Δ30; for 2070–2099 less 2001–2030) for $H_{99}$ (M = 4) and $H_{90}$ (Figs. 11, 12, respectively) can be compared to the corresponding results from the wave model (Figs. 6, 7). Consistent with the low values of $S_{PAT}$ and better values of $R_{PAT}$ in Table 2, these results show that although the statistical projections provide a qualitative idea of the modeled patterns twenty-first century changes, the magnitudes of the projected changes are typically only ~30–50 % as large as those from the wave model results. The statistical projections for $H_{99}$ are particularly muted in comparison to the wave model results, and note that the modeled increases in wave heights across the high latitude central North Pacific and Gulf of Alaska are essentially absent from the statistical results. To give an idea of changes through time at one location, Fig. 13 compares the time series of dynamically and statistically modeled $H_{90}$ at 30 N 170E and clearly shows that the statistical results do not fully track the evolving trend towards lower wave heights during the twenty-first century. This behavior is emphasized by frequency distributions (Fig. 14) for the dynamical and statistically-derived data for (1) 2001–30 and (2) 2070–2099. The distributions agree fairly well in the former period, but are distinct in the latter decades as the dynamically-modeled wave heights increasingly diverge from late twentieth century conditions.

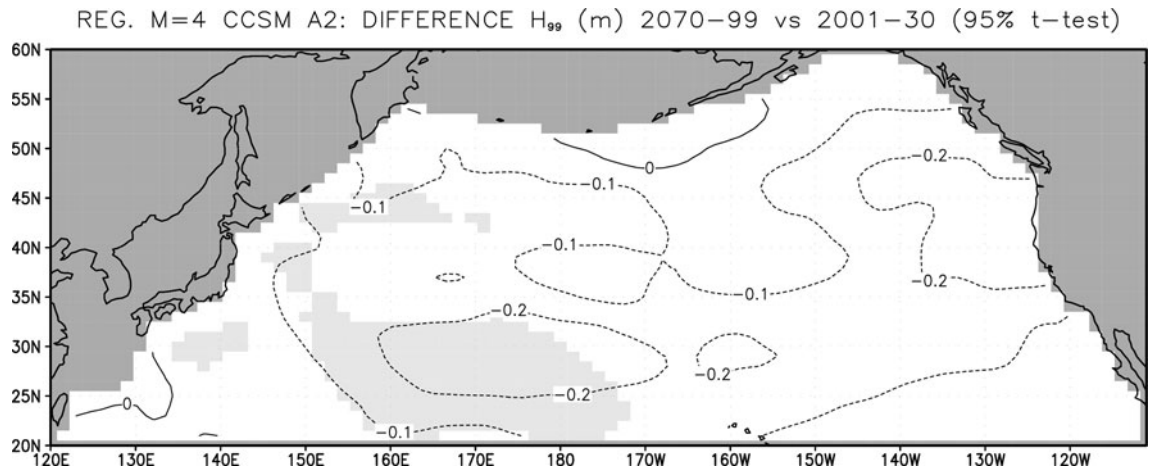


**Fig. 11** Differences (m) in statistically-derived winter average $H_{99}$ (2070–2099 less 2001–2030) for CCSM-A2. Results shown here, for M = 4 retained EOF modes, agreed best with the numerically-derived differences (Fig. 6a) in terms of pattern skill ($S_{PAT}$). *Shading* (*hatching*) indicates where differences exceed the *t* test 95 % confidence limit

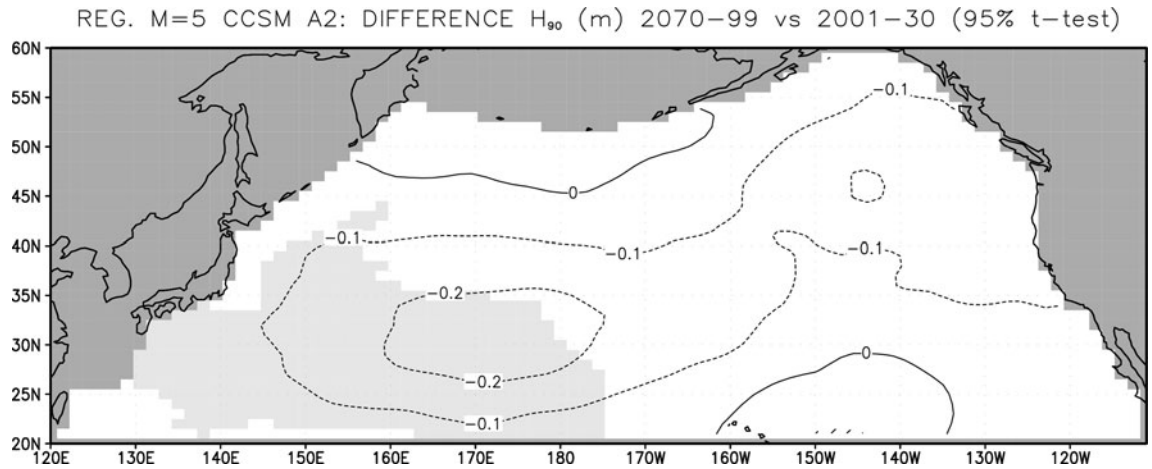


**Fig. 12** Differences (m) in statistically-derived winter average $H_{90}$ (2070–2099 less 2001–2030) for CCSM-A2. Results shown here, for M = 5 retained EOF modes, agreed best with the numerically-derived differences (Fig. 7a) in terms of pattern skill ($S_{PAT}$). *Shading* (*hatching*) indicates where differences exceed the *t* test 95 % confidence limit

Several factors limit the performance of the statistical models described above. These include:

1. The limited hindcast performance (i.e., the performance over the training period) of the statistical models. While the hindcast skill is inflated somewhat by "artificial skill" (see below), if taken as a rough estimate of forecast skill it explains a substantial part of the difference between the statistically-derived and modeled Δ30 maps. For example, projecting the $H_{90}$ hindcast correlation map (Fig. 10b) onto the $H_{90}$ Δ30 values (Fig. 7) produces the pattern shown in Fig. 15. While this result agrees more closely with the dynamical results (Fig. 7) than do the statistical model projections (Fig. 12), considerable variability is lost. Corresponding results for $H_{99}$ (not shown) are similar in pattern and magnitude to those in Fig. 12, emphasizing that it is lower hindcast skills for $H_{99}$ are largely responsible for the similarity between the statistically-derived $H_{90}$ and $H_{99}$ Δ30 maps (Figs. 11, 12).
2. Associations between random fluctuations in the SLP and wave quantile fields over the hindcast period produce errors in the estimated statistical models and a high bias in hindcast skill ("artificial skill"); this will result in a tendency for errors during the "forecast period" to exceed those in the "training period". This effect is apparent in the time series of map-averaged RMS differences between the statistical and dynamical model $H_{99}$ (Fig. 16) in which the average error for the forecast period is about 10 % higher than in the training period. The effect is not nearly so clear for $H_{90}$ (not shown).

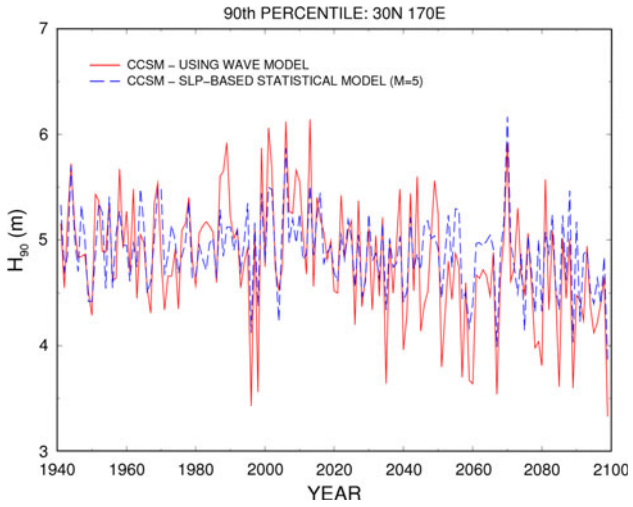


**Fig. 13** Time series of $H_{90}$ (m) at 30 N 170E from the wave model (*red*) using CCSM forcing (*red solid line*) and "best" (in terms of twenty-first century pattern skill; M = 5, see text) statistical model (*blue dashed line*) trained over 1941–2000

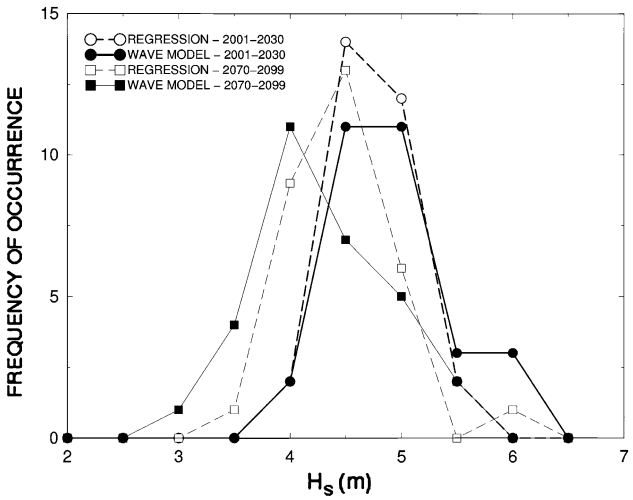


**Fig. 14** Frequency distributions for $H_{90}$ (m) at 30 N 170E from CCSM-forced wave model and best statistical model (in terms of twenty-first century pattern skill, M = 5) trained over 1941–2000. Results for 2001–2030 are shown by *heavy solid line with filled circles* (wave model) and *heavy dashed line with open circles* (statistical model); results for 2070–2099 are shown by *light solid line with filled squares* (wave model) and *light dashed line with open squares* (statistical model)

3. Non-stationarity in physical processes and relationships related to the changing climate could also result in degradation of statistical model "forecast" skill though time. This effect may be difficult to separate unambiguously from artificial skill described above, but would be most obviously shown by trends in errors through the twenty-first century. The fact that the RMS errors plotted in Fig. 15 show little trend after the beginning of the forecast period (after the year 2000) suggests that the relationships between seasonal mean SLP and upper wave height quantiles (like those embodied in the statistical model coefficients) are not changing a great deal as the twenty-first century progresses (the same is true of $H_{90}$).

As a final note, we also tested regression models like those described above using $WS_{90}$ rather than mean SLP as the predictor field for $H_{90}$. The best of models in terms of 30-year twenty-first century differences ($\Delta$) showed performance levels similar to those found using mean SLP as the predictor field.

## 4 Summary and discussion

A third generation wave model, Wavewatch III, has been run over the North Pacific Ocean poleward of 20 N over the twenty-first century using near-surface winds from three CGCMs (CCSM, CNRM, EH4) under the IPCC A2 emissions scenario. Results are analyzed for boreal winter (November–March), the period when North Pacific storminess and wave energy is greatest. The CGCM near-surface winds were adjusted to bring the modern CGCM-derived wave climatologies into better agreement with those obtained using NCEP-RA winds. These adjustments were made using a vertical wind profile approach that modifies the CGCM wind speed by altering the nominal "observation" height for the CGCM winds. Once selected, the adjustment in "observation" height for a given CGCM are fixed in time and space, producing changes in relative (fractional) wind speed adjustments that vary by at most a few percent for wind speeds above 10 $ms^{-1}$. The resulting changes in wind speeds are rather small in comparison to the total wind speed, so the basic spatial and temporal patterns of wind field variability for each CGCM are approximately preserved.

To compare with the numerical model results, a commonly used statistical methodology (e.g. WASA98; WS2001; WS2002; WZS2004) for estimating seasonal wave height quantiles on the basis of seasonal mean SLP was applied using results from one of the CGCMs (CCSM). Statistical models were trained over the last 60 years of the twentieth century and applied to provide projections for the twenty-first century.

The findings from our work bear on a range of key science questions that have been identified related to projections of future wave climate (Hemer et al. 2012b). These include methods for transforming CGCM wind fields into products more directly comparable with reanalysis results, the use of dynamical wave models with CGCM-derived wind fields, the character of CGCM-projected changes in near-surface circulation and their effects on wave climate,

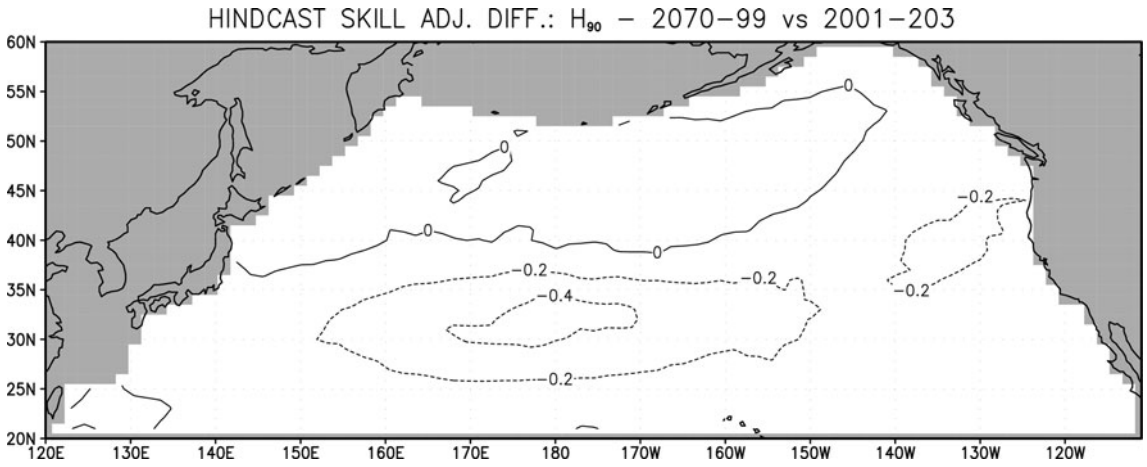


**Fig. 15** Projection of statistical model hindcast correlations (square root of model $R^2$) for $H_{90}$ (m = 5; Fig. 10b) onto the $H_{90}$ wave model-derived Δ30 pattern (Fig. 7). These results show what the corresponding statistical model Δ30 pattern would look like if statistical hindcast skill was preserved through the twenty-first century (compare with Fig. 12)

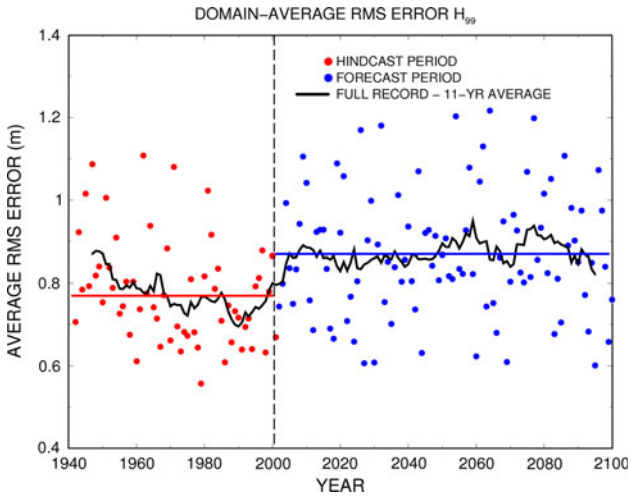


**Fig. 16** Winter domain-averaged $H_{99}$ root-mean-square error (wave model vs. statistical model). *Red* and *blue circles* show values for individual years in the hindcast and forecast periods, respectively; *red* and *blue lines* show the overall averages for the hindcast and forecast periods, respectively; *black curve shows* the 11-year running mean; *dashed vertical line* separates the hindcast and forecast periods

and the performance of statistical models to produce wave climate projections.

The main findings from the study are discussed below.

1. After the adjustments to the large-scale wind field noted above, the CGCM simulated patterns of 90th percentile winds ($WS_{90}$, $\mathbf{U}_{90}$) and 99th percentile wave heights ($H_{99}$, $\mathbf{D}_{99}$) for the modern period show good agreement in pattern and reasonable agreement in magnitude with those obtained from NCEP-RA results.
2. Over the twenty-first century, the wave model results from the three CGCMs show similar patterns of change. All three simulations yield statistically significant and widespread decreases in $H_{90}$ and $H_{99}$ across the lower mid-latitudes (south of ~40 N) of the western and central North Pacific. In this region, the declines in $H_{99}$ range from ~0.75–1.5 m (10–15 %). All three models show less widespread, but statistically significant increases (up to 0.5 m, ~5 %) in $H_{99}$ across parts of the high latitude central and eastern North Pacific, but only one model shows significant increases in $H_{90}$.
3. The twenty-first century decreases in wave heights across the lower mid-latitudes are associated with statistically significant decreases in 90th percentile windspeeds (~0.75–1.0 $ms^{-1}$, ~5–7 %). These declines are described better as confined to the zone of strong wind speed gradients along the southern flank of the main core of westerlies rather than reflecting a northward shift of the entire circulation pattern.
4. At higher latitudes, the simulated increases in $H_{99}$ are not associated with the same pattern of change in winds in all of the models. In CCSM, neither $WS_{90}$ nor $WS_{99}$ show more than small increases; in CNRM, the increased wave heights are associated with increases in both $WS_{90}$ and $WS_{99}$; and in EH4, $WS_{99}$ increases and $WS_{90}$ does not. Thus, the increases in high latitude $H_{99}$ can be attributed to different factors in the three simulations: general increases in upper quantiles of windspeeds (CNRM), increases in windspeeds only in the highest quantiles (EH4), or possibly changes in cyclone tracks that are more favorable for generating waves that affect high latitude northeast Pacific (CCSM).
5. Along the coast of the western North America, the CGCM results (Figs. 6, 7) show a general pattern of decreased twenty-first century wave heights to the south tending towards positive changes farther north, though spatial details, magnitudes and statistical

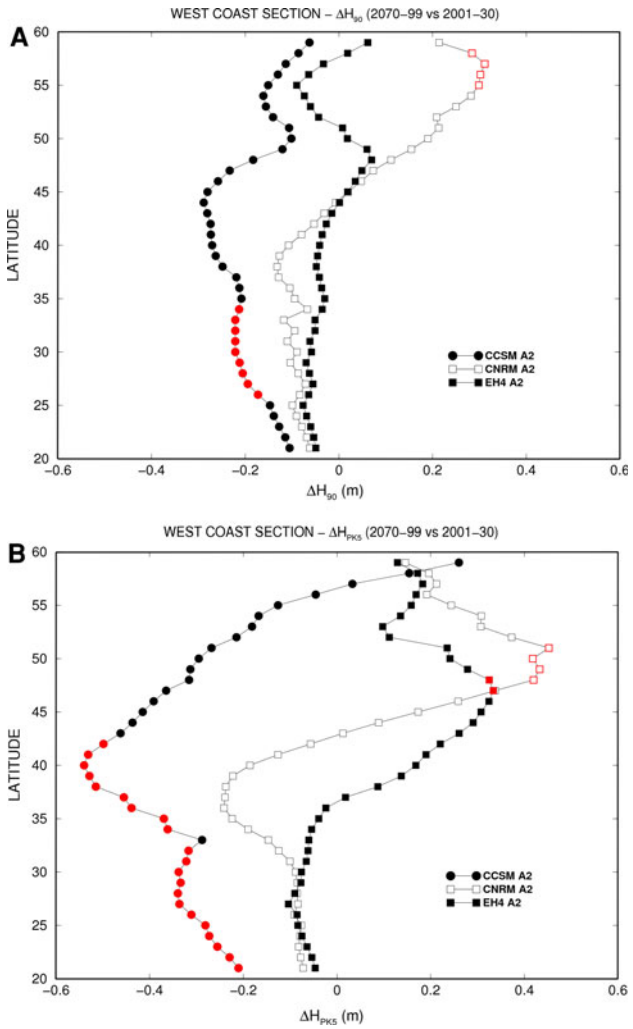


**Fig. 17** West coast North America sections of twenty-first century differences (2070–2099 vs. 2001–2030) in $H_{90}$ (**a**) and $H_{PK5}$ (**b**) for CCSM (*filled circles*), CNRM (*open circles*) and EH4 (*filled squares*). *Red symbols* indicate locations where differences exceed the 95 % *t* test significance level; see Fig. 7a for locations

significance vary from model to model, and with the wave height statistic used. To provide more detail, Fig. 17 shows latitudinal profiles of 2070–2099 versus 2001–2099 differences in $H_{90}$ and $H_{PK5}$ (see Sect. 2.3.1; also Fig. 7a for locations). This general pattern is the inverse of that found in hindcasts for the late twentieth century (e.g. WS2001; Graham 2005), and measured (buoy) wave height records covering the past few decades which show positive trends south of ~40–45 N and negative trends to the north (e.g., Ruggiero et al. 2010; Gemmrich et al. 2011). Further, the maximum absolute changes in simulated $H_{PK5}$ along the west coast transect (~0.5 m over 70 years, or ~7 mm year$^{-1}$; Fig. 17b) are much smaller than some reported trends in $H_{PK5}$ derived from buoy data in the Northeast Pacific (e.g., Ruggiero et al. 2010), though recent work suggests that the buoy-derived trends may be substantially affected by changes platform design, instrumentation and data processing through the years (Gemmrich et al. 2011)].

6. Statistical models based on winter mean SLP (and trained through the latter half of the twentieth century) were able to qualitatively reproduce the CCSM simulated pattern of decreased $H_{90}$ and $H_{99}$ wave heights across the lower mid-latitudes during the twenty-first century. However, the statistical models typically underestimated the magnitude of the changes by 50 % or more, particularly for $H_{99}$, and did not capture the high latitude increases in $H_{99}$ found in the dynamical model results. Diagnostic analysis reveals that the relatively poor performance of the CCSM-derived statistical models is due largely to low hindcast skill in the statistical models, with errors in the estimated statistical models also contributing. There is little clear evidence that secular changes in the physical relationships relating mean seasonal SLP to wave heights played an important role, though our analyses do not rule this out. Further, it should be kept in mind that while our statistical results should have some broad relevance, they are germane only to a single CGCM simulation and one statistical method.

Relatively few studies relating to projected changes in winter century wave climate across the North Pacific during the twenty-first century are available for comparison with our results. Wang and Swail (2006) used reanalysis results and reanalysis-driven wave model output to develop pointwise regression and extreme-value models for winter average $H_S$ and 20-year return periods (respectively) based on seasonal SLP and squared SLP gradients. These models were then implemented using SLP from three different CGCMs (CGCM2, Hadley Centre HADCM2, and EH4) run under three different IPCC emissions scenarios, including the A2 scenario treated in this paper. Although not directly comparable to ours, the spatial pattern for the combined A2 results resembles those we find over the western half of the North Pacific, but the magnitudes of the declines in their projected changes are only about 10 % of those for average $H_S$ seen in the models we used (0.3–0.5 m; not shown). The patterns of change in the eastern North Pacific are quite different to those we find. In related work, Caires et al. (2006) used a different extreme value model trained with reanalysis data and applied it to CGCM2 A2 data to estimate changes 20-year return $H_S$ on the basis of seasonal SLP and squared SLP gradients. The patterns of winter wave height change indicated in their results are similar to those of Wang and Swail (2006).

As noted in the Introduction, Mori et al. (2010; see their Fig. 3) used winds from an atmospheric climate model driven with average SSTs from a multi-model ensemble of IPCC A1B scenario simulations (A1B is a "middle of the road" emissions scenario) to drive a global numerical wave model through the twenty-first century. Though the results they show are for annual average $H_S$, the pattern of change over the North Pacific (which is likely dominated by boreal winter results) closely resembles those seen in our results (Figs. 6, 7) with 5–10 % decreases across the lower mid-latitudes of the North Pacific and smaller increases at higher latitudes across the western and central ocean.

In contrast to the paucity of studies of twenty-first century wave climate changes in the North Pacific, there are numerous studies relating to changes in winter cyclone activity and occurrence of strong winds. Consistent with our results, many of these indicate decreases in these indices across the lower mid-latitudes and increases farther north. These include analyses of the frequency of strong winds (Fischer-Bruns et al. 2005), cyclone track, intensity and frequency (Yin 2005; Bengtsson et al. 2006; Favre and Gershunov 2009), eddy kinetic energy (Laíne et al. (2009), and band-passed SLP (Ulbrich et al. 2009). Other analyses from our work concerning the frequency of occurrence of strong winds and changes in band-passed SLP variability (not shown) give results consistent with those in the first and the last citations above, and qualitatively with the simulated patterns of change in wave heights.

It is natural to consider whether changes in winter North Pacific wave heights similar to those presented here can be detected in hindcasts results and buoy measurements from recent decades. On this point, given the presence of multi-decadal variability (e.g., Fig. 13) and from the contrast between projected results and recent observed changes brought out in the discussion above (Point 5), the conclusion would appear negative. On the other hand, trends in wave heights (annual average and $H_{90}$) from satellite measurements over 1985–2008 (Young et al. 2011) show some similarity to our results, in particular in indicating a downward trend ($\sim -0.25$ % year$^{-1}$) across the lower mid-latitudes of the central North Pacific. For comparison, the CCSM results for November–March $H_{90}$ at 30 N 170E (see Figs. 7, 13) give a value for the twenty-first century of $\sim -0.14$ % year$^{-1}$. Using this simulated record for 1985 forward, the significance of the downward (linear) trend would reach the 95 % level by $\sim$2040–2050 (not shown). Thus, if the simulated changes are approximately correct, it will be a few decades yet before the changes in North Pacific wave climate due to increasing greenhouse gas concentrations are clearly detectable.

**Acknowledgments** This work was conducted under funding from the California Energy Commission PIER Program through a University of California, California Institute for Energy and Environment (UC-CIEE) Award, No. POCV01-X12 to Scripps Institution of Oceanography (DC, PB, RF) and sub-award 500-09-038 to the Hydrologic Research Center (NG). The authors extend many thanks to Emelia Bainto and Mary Tyree for their valuable assistance with the wave model simulations, and with data acquisition and processing. Thanks as well to three anonymous reviewers whose suggestions helped improve the manuscript.

## Appendix 1: PC regression and twenty-first century wave climate projections

Empirical orthogonal functions (EOFs) of the predictor (Y; mean November-March SLP over the North Pacific and surrounding region) and predictand (Z; modeled November–March North Pacific $H_{90}$ or $H_{99}$) are obtained from their respective variance-covariance matrices as shown below,

$$C_{YY}e = \kappa e \quad (1)$$

$$C_{ZZ}f = \lambda f \quad (2)$$

where $C_{YY}$ ($C_{ZZ}$) is the variance-covariance matrix, e(f) is an orthonormal matrix of eigenvectors (or "loadings") and $\kappa(\lambda)$ is a diagonal matrix of eigenvalues for the predictor (predictand) variable. Note that in the notation here Y and Z represent anomalies from their respective means over the training period. The predictor and predictor data for the CCSM analyses are for 1941–2000 (notation referring to the ending year of the winter season). Data up to December 1999 come from the CCSM 20C3M simulations (CGCM for SLP, wave model simulations for wave heights) and for January–March come from the CCSM A2 simulations. An analogous exercise, designed to help evaluate the statistical model regression results derived from CCSM, was conducted using NCEP-RA winds and the wave measures obtained from a historical run of WW3 driven by NCEP-RA winds for the 1948–1999 period.

The EOF PCs, $\alpha$ and $\beta$, obtained by projecting the (orthonormal) loadings onto the original data,

$$\alpha = Ye \quad (3)$$

$$\beta = Zf \quad (4)$$

carry the variance of the respective EOF modes, so that

$$\left\langle \alpha_i^2 \right\rangle = \kappa_i \quad (5)$$

$$\left\langle \beta_j^2 \right\rangle = \lambda_j \quad (6)$$

where the angle brackets indicate an expectation, $\kappa$ and $\lambda$ are eigenvalues and subscripts indicate the EOF mode number.

From this point, linear least-squares regression weights (A) are obtained via

$$A = (\alpha^t\alpha)^{-1}(\alpha^t\beta) \quad (7)$$

Then

$$\beta^* = \alpha A \quad (8)$$

gives hindcast estimates (indicated by the asterisk) of the predictand PCs for the training period, and projection onto the predictand loadings converts these back into full fields in their original units,

$$Z^* = \beta^* f^t \quad (9)$$

The fraction of total hindcast predictand variance accounted for by the regression is then

$$R^2 = \mathrm{Tr}(Z^*Z^{*t})\mathrm{Tr}(ZZ^t)^{-1} \quad (10)$$

while

$$RI = \mathrm{Tr}\left(\beta^*\beta^{*t}\right)\mathrm{Tr}\left(\beta\beta^t\right)^{-1} \quad (11)$$

is a "redundancy index" (e.g., WS2001, WS2004), and gives the fraction of EOF-truncated variance retained by the regression.

To make projections (indicated by the super-script "p") of future wave conditions ($Z^p$), the predictor EOF loadings are projected onto the simulated (projected) twenty-first century SLP fields ($Y^p$) yielding "pseudo-PCs"

$$A^p = Y^p e^t \quad (12)$$

for 2001–2099. Then, following from Eqs. 8 and 9,

$$\beta^p = \alpha^p A \quad (13)$$

and

$$Z^p = \beta^p f^t \quad (14)$$

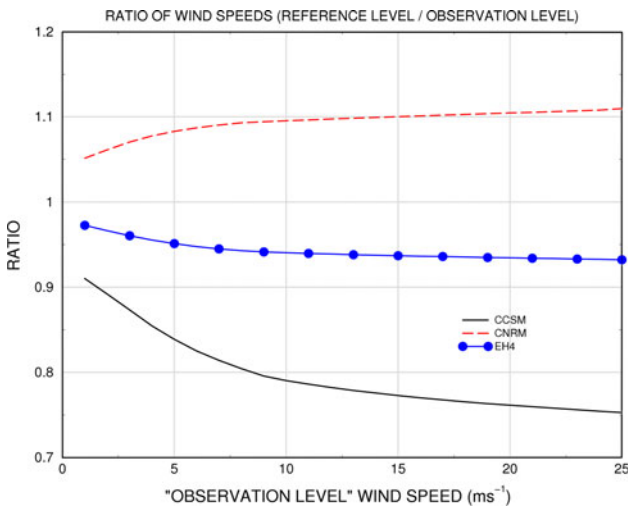


**Fig. 18** Ratio of adjusted (reference level) to unadjusted (observation level) CGCM near-surface wind speeds as a function of unadjusted wind speed; CCSM *solid black line*, CNRM *red dashed line*, EH4 *solid blue line with circles*

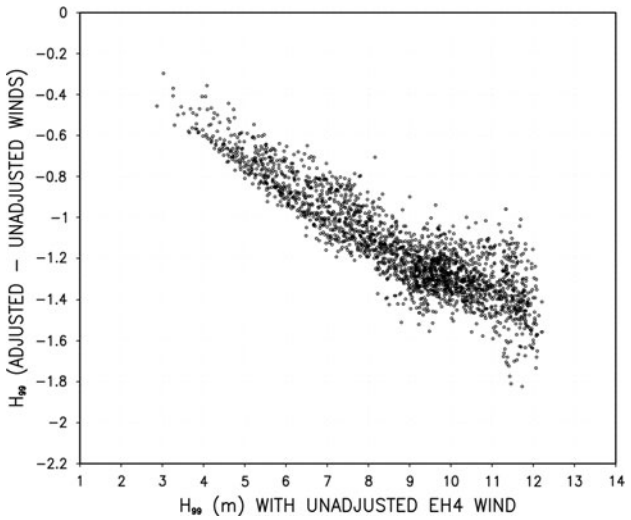


**Fig. 19** Example of wave height changes resulting from wind speed adjustments. Difference in mean November–March EH4 winter average $H_{99}$ for 1990–1992 (with less without wind speed adjustments) plotted as a function of $H_{99}$ without adjustment; all locations in the model domain are plotted. The downward adjustments in reference level wind speed ($\sim$6–7 % for wind speeds $> 10$ ms$^{-1}$; Fig. 18) yield approximately linear (14 %) decreases in $H_{99}$

give the regression-based estimates of future values of the predictand PCs ($\beta^p$), and finally of the predicatand ($Z^p$) by projection onto the predictand loadings (f). The training period means for Z can be then added back to $Z^p$ if desired.

## Appendix 2

Supplementary figures related to model CGCM wind speed adjustments and example of resulting changes in wave heights (Figs. 18, 19).

## References

Adams PN, Inman DL, Graham NE (2008) Southern California deep-water wave climate: characterization and application to coastal processes. J Coast Res 24:1022–1035

Alexander M, Yin J, Branstator G, Capotondi A, Cassou C, Cullather R, Kwon Y-O, Norris J, Scott J, Wainer I (2006) Extratropical atmosphere-ocean variability in CCSM3. J Clim 19:2496–2525

Allan JC, Komar PD (2000) Are ocean wave heights increasing in the eastern N. Pacific? EOS Trans Am Geophys Union 47:561–567

Bacon S, Carter DJT (1991) Wave climate changes in the North Atlantic and North Sea. Int J Climatol 11:545–558

Bacon S, Carter DJT (1993) A connection between mean wave height and atmospheric pressure gradient in the North Atlantic. Int J Climatol 13:423–436

Barnett TP, Latif M, Graham N, Flugel M, Pazan S, White W (1993) ENSO and ENSO-related predictability: Part 1 Prediction of

equatorial Pacific sea surface temperatures with a hybrid coupled ocean-atmosphere model. J Clim 6:1545–1566
Bengtsson L, Hodges K, Roeckner E (2006) Storm tracks and climate change. J Clim 16:3518–3543
Bouws E, Jannick D, Komen GR (1996) Increasing wave height in the North Atlantic. Bull Am Meteorol Soc 77:2275–2277
Bromirski PD, Cayan DR, Flick RE (2005) Wave spectral energy variability in the Northeast Pacific Ocean. J Geophys Res 110:C03005. doi:10.1029/2004JC002398
Caires S, Sterl A, Bidlot J-R, Graham N, Swail V (2004) Intercomparison of different wind-wave reanalyses. J Clim 17:1893–1913
Caires S, Swail VR, Wang XL (2006) Projections and analysis of extreme wave data. J Clim 19:5581–5605
Carter DJT, Draper L (1988) Has the northeast Atlantic become rougher? Nature 332:494
Cayan DR, Tyree M, Dettinger M, Hidalgo H, Das T, Maurer E, Bromirski P, Graham N, Flick R (2009) Climate change scenarios and sea level rise estimates for the California 2008 climate change scenarios assessment. California Energy Commission, PIER Energy-Related Environmental Research, 62 p. CEC-500-2009-014. Available on-line: http://www.energy.ca.gov/2009publications/CEC-500-2009-014/CEC-500-2009-014-D.PDF
Chang EKM, Fu Y (2003) Using mean flow change as a proxy to infer interdecadal storm track variability. J Clim 16:2178–2196
Collins WD et al (2006a) The community climate system model version 3 (CCSM3). J Clim 19:2122–2143
Collins WD, Rasch PJ, Boville BA, Hack JJ, McCaa JR, Williamson DL, Briegleb PB, Bitz CM, Lin S-J, Zhang M (2006b) The formulation and atmospheric simulation of the Community Atmosphere Model: CAM3. J Clim 19:2144–2161
Cox A, Swail V (2001) A global wave hindcast over the period 1958–1997: validation and climate assessment. J Geophys Res 106:2313–2329
Favre A, Gershunov I (2009) North Pacific cyclonic and anticyclonic transients in a global warming context: possible consequences for Western North American daily precipitation and temperature extremes. Clim Dyn 32:969–987
Fischer-Bruns I, von Storch H, Gonzales-Rouco JF, Zorita E (2005) Modelling the variability of midlatitude storm activity on decadal to century time scales. Clim Dyn 25:461–476
Flato GM, Boer GJ (2001) Warming asymmetry in climate change simulations. Geophys Res Lett 28:195–198
Gemmrich J, Thomas B, Bouchard R (2011) Observational changes and trends in northeast Pacific wave records. Geophys Res Lett 38:L22601. doi:10.1029/2011GL049518
Gibson JK, Kållberg P, Uppala S, Hernandez A, Nomura A, Serrano E (1997) ERA description. Vol 1, ECMWF re-analysis, ECMWF Project Report Series, 72 p
Graham NE (1993) Decadal-scale climate variability in the tropical and North Pacific during the 1970's and 1980's: observations and model results. Clim Dyn 10:135–162
Graham NE (2005) Coastal impacts of North Pacific winter wave climate variability: the Southern California Bight and the Gulf of the Farallones. Scripps Institution of Oceanography, for the California Energy Commission, PIER Energy Related Environmental Research, CEC-500-2005-018. Available at: http://www.energy.ca.gov/2005publications/CEC-500-2005-018/CEC-500-2005-018.PDF
Graham NE, Diaz H (2001) Evidence for intensification of North Pacific winter cyclones since 1948. Bull Am Meteorol Soc 82:1869–1893
Gulev SK, Grigorieva V (2004) Last century changes in ocean wind wave height from global visual wave data. Geophys Res Lett 31:L24302. doi:10.1029/2004GL021040
Gulev SK, Grigorieva V (2006) Variability of the winter wind waves and swell in the North Atlantic and North Pacific as revealed by the Voluntary Observing Ship data. J Clim 19:5667–5685
Günther H, Rosenthal W, Stawarz M, Carretero JC, Gomez M, Lozano I, Serano O, Reistad M (1998) The wave climate of the Northeast Atlantic over the period 1955–94: the WASA wave hindcast. Glob Atmos Ocean Syst 6:121–163
Hemer MA, McInnes KL, Ranasinghe R (2012) Climate and variability bias adjustment of climate model derived winds for an east Australian dynamical wave model. Ocean Dyn 62:87–104. doi:10.1007/s10236-011-0486-
Hemer MA, Wang XL, Weisse R, Swail VR, and the COWLIP team (2012b) Community advancing wind-waves climate science: The COWCLIP project. Bull Am Meteorol Soc. doi:10.1175/BAMS-D-11-00184.1
Horel JD (1981) A rotated principal component analysis of the interannual variability of the Northern Hemisphere 500 mb height field. Mon Weather Rev 109:2080–2092
Hotelling H (1957) The relationship of the newer multivariate statistical methods to factor analysis. Br J Stat Psychol 10:69–79
Hurrell JW (1995) Decadal trends in the North Atlantic oscillation: regional temperatures and precipitation. Science 269:676–679
Jolliffe LT (2002) Principal component analysis, 2nd edn. Springer, New York, pp 167–195, 487 pp + illustrations
Kaas E, the STOWASUS Group (2001) Regional storm, wave and surge scenarios for the 2100 century (STOWASUS-2100). Final report. Available online at http://www.dmi.dk/pub/STOWASUS-2100/
Kalnay E, Kanamitsu M, Kistler R, Collins W, Deaven D, Gandin L, Iredell M, Saha S, White G, Woollen J, Zhu Y, Chelliah M, Ebisuzaki W, Higgins W, Janowiak J, Mo KC, Ropelewski C, Wang J, Leetmaa A, Reynolds R, Jenne R, Joseph D (1996) The NMC/NCAR 40-year reanalysis project. Bull Am Meteorol Soc 77:437–471
Kendall MG (1957) A course in multivariate analysis. Griffin, London
Kiehl JT, Shields CA, Hack JJ, Collins WD (2006) The climate sensitivity of the community climate system model version 3 (CCSM3). J Clim 19:2584–2596
Kushnir Y, Cordone VJ, Greenwood JG (1997) The recent increase in North Atlantic wave heights. J Clim 10:2107–2113
Kvamstø NG, Song Y, Seierstad IA, Sorteberg A, Stephenson DB (2008) Clustering of cyclones in the ARPEGE general circulation model. Tellus A 60:547–556
Laíne A, Kageyama M, Salas D, Ramstein G, Planton S, Denvil S, Tyteca S (2009) An energetics study of winter-time northern hemisphere storm tracks under 4 × CO_2 conditions in two ocean-atmosphere coupled models. J Clim 22:819–839
Lambert SJ, Fyfe JC (2006) Changes in winter cyclone frequencies and strengths simulated in enhanced greenhouse warming experiments: results from the models participating in the IPCC diagnostic exercise. Clim Dyn 26:713–728
Lau N-C (1988) Variability of the observed midlatitude storm tracks in relation to low-frequency changes in the circulation pattern. J Atmos Sci 45:2718–2743
Legutke S, Voss R (1999) The Hamburg atmosphere-ocean coupled circulation model. DKRZ Technical Report No. 18, Deutsches KlimaRechenZentrum, Hamburg, 61 p
Liu WT, Katsaros KB, Businger JA (1979) Bulk parameterization of air-sea exchange of heat and water vapor including the molecular constraints of the interface. J Atmos Sci 36:1722–1735
Mizuta R, Yukimasa A, Yukimoto S, Kusunoki S (2008) Estimation of the future distribution of sea surface temperature and sea ice using CMIP3 multi-model ensemble mean. Tech. Rep. Meteor. Res. Inst., 56, 28 pp
Mori N, Yasuda T, Mase H, Tracey T, Oku Y (2010) Projection of extreme wave climate change under global warming. Hydrol Res Lett 4:15–19
Nakicenovic N et al (2000) Special report on emissions scenarios: a special report of working group III of the intergovernmental panel

on climate change. Cambridge University Press, Cambridge, 599 p. Available online at: http://www.grida.no/climate/ipcc/emission/index.htm

Ruggiero P, Komar PD, Allan JA (2010) Increasing wave heights and extreme value projections: the wave climate of the U.S. Pacific Northwest. Coast Eng 57:539–552

Salas-Mélia D, Chauvin F, Déqué M, Douville H, Gueremy JF, Marquet P, Planton S, Royer JF, Tyteca S (2005) Description and validation of the CNRM-CM3 global coupled model. CNRM working note 103

Sokal RR, Rohlf FJ (1969) Introduction to biostatistics. W.H. Freeman, San Francisco

Stendel M, Roeckner E (1998) Impacts of horizontal resolution on simulated climate statistics in ECHAM4. Report no. 253, Max-Planck-Institut für Meteorologie, Bundesstr 55, Hamburg, 55 pp

Swail VR, Cox AT (2000) On the use of NCEP-NCAR reanalysis surface marine wind fields for a long-term North Atlantic wave hindcast. J Atmos Ocean Technol 17:77–86

Tolman HL (1999) User manual and system documentation of WAVEWATCH III, version 1.18, US Dept. of Commerce, NOAA, NWS, NCEP, Ocean Modeling Branch Contribution 166, 4700 Silver Hill Road, Mail Stop 9910, Washington, D.C. 20233-9910, 112 p

Tolman HL (2003) Treatment of unresolved islands and ice in wind wave models. Ocean Model 5:219–231

Trenberth KE (1990) Recent observed interdecadal climate changes in the northern hemisphere. Bull Am Meteorol Soc 71:988–993

Trenberth KE, Hurrell JW (1994) Decadal atmosphere-ocean variations in the pacific. Clim Dyn 9:303–319

Tyler DE (1982) On the optimality of the simultaneous redundancy transformations. Psychometrika 47:77–86

Ulbrich U, Pinto JG, Kupfer H, Leckebusch GC, Spangehl T, Reyers M (2008) Changing Northern Hemisphere storm tracks in an ensemble of IPCC climate change simulations. J Clim 21:1669–1679

Ulbrich U, Leckebusch G, Pinto J (2009) Extra-tropical cyclones in the present and future climate: a review. Theor Appl Climatol 96:117–131

Uppala SM et al (2005) The ERA-40 re-analysis. Q J R Meteorol Soc 131:2961–3012

von Storch H, Zweirs FW (1999) Statistical analysis in climate research. Cambridge University Press, Cambridge

Wang XL, Swail VR (2001) Changes in extreme wave heights in the Northern Hemisphere Oceans and related atmospheric circulation regimes. J Clim 14:2204–2221

Wang XL, Swail VR (2002) Trends of Atlantic wave extremes as simulated in a 40-yr wave hindcast using kinematically reanalyzed wind fields. J Clim 15:1020–1035

Wang XL, Swail VR (2006) Climate change signal and uncertainty in projections of ocean wave height. Clim Dyn 26:109–126

Wang XL, Zwiers FW, Swail VR (2004) North Atlantic Ocean wave climate change scenarios for the 21st century. J Clim 17:2368–2383

Wang XL, Swail VR, Cox A (2010) Dynamical versus statistical downscaling methods for ocean wave heights. Int J Climatol 30:317–332

WASA Group (1998) Changing waves and storms in the Northeast Atlantic? Bull Am Meteorol Soc 79:741–760

Woolf DK, Challenor PG, Cotton PD (2002) The variability and predictability of North Atlantic wave climate. J Geophys Res 107:3145. doi:10.1029/2001JC001124

Yin JH (2005) A consistent poleward shift of the storm tracks in simulations of 21st century climate. Geophys Res Lett 32:L18701. doi:10.1029/2005GL023684

Young IM, Zieger S, Babanin V (2011) Global trends in wind speed and wave height. Science 332:451–455

Zhu X, Sun J, Liu Z, Liu Q, Martin JE (2007) A synoptic analysis of the interannual variability of winter cyclone activity in the Aleutian low region. J Clim 20:1523–1538